

Event-by-event azimuthal anisotropy of jet quenching in relativistic heavy ion collisions

Xilin Zhang^{1,3*} and Jinfeng Liao^{1,2†}

¹ *Physics Department and Center for Exploration of Energy and Matter,
Indiana University, 2401 N Milo B. Sampson Lane, Bloomington, IN 47408, USA.*

² *RIKEN BNL Research Center, Bldg. 510A,
Brookhaven National Laboratory, Upton, NY 11973, USA.*

³ *Institute of Nuclear and Particle Physics and Department of Physics and Astronomy,
Ohio University, Athens, OH 45701, USA.*

(Dated: April 21, 2013)

Abstract

Background: Strong jet quenching has been observed in heavy ion collisions at both the Relativistic Heavy Ion Collider (RHIC) and the Large Hadron Collider (LHC) that can be understood through substantial jet energy loss in the created hot QCD matter. Yet the azimuthal anisotropy of jet quenching has not been thoroughly studied in the presence of strong fluctuations in the initial condition.

Purpose: We present with full details a systematic quantification of the hard probe azimuthal response to the geometry and fluctuations of the hot QCD matter at both RHIC and LHC. We also examine the hard-soft dihadron correlation arising from the hard and soft sectors' responses to the common fluctuating initial condition.

Methods: An even-by-event MC simulation is employed. Different geometrical jet-quenching models are tested. The azimuthal anisotropy of jet quenching is extracted and decomposed as harmonic responses (for $n=1-6$) to the corresponding harmonics in the initial state.

Results: We show that such jet response harmonics are sensitive to the jet quenching models as well as to the initial composition of bulk matter. Their centrality dependence puts a strong constraint on the path-length and medium-density dependence of jet energy loss. The computed hard-soft dihadron correlation shows a strong peak on the near side in RHIC central collisions. The triggered correlation in noncentral collisions is also presented.

Conclusions: Only the jet-quenching model with near- T_c enhancement survives the second-harmonic test by the RHIC and LHC. Other harmonics in this model are consistent with the available data. We also demonstrate that the experimentally observed “hard ridge” can be explained in our calculation and that its trigger-azimuthal-angle and associate- p_t dependence could also be qualitatively understood.

PACS numbers: 25.75.-q, 12.38.Mh

*Electronic address: zhangx4@ohio.edu

†Electronic address: liaoji@indiana.edu

I. INTRODUCTION

In high energy nucleus-nucleus (AA) collisions, the hot deconfined QCD matter, so-called quark-gluon plasma (QGP), is believed to be created at both the Relativistic Heavy Ion Collider (RHIC) and the Large Hadron Collider (LHC). Also created in such collisions are jets from the initial hard scatterings, which penetrate the soft matter and eventually convert into hadrons. Along its path through the medium, the jet keeps interacting with the medium and losses energy. The quenching of jets due to the energy loss can be used to characterize the jet-medium interaction as well as the medium properties, which provides an imaging tool of QGP often called jet tomography (see, e.g., reviews in Refs. [1]).

A traditional single hadron observable for quantifying the jet quenching is the so-called nuclear modification factor R_{AA} , i.e., the ratio between the hadron production in AA collisions and that in NN collisions (multiplied by the expected binary collision number). In the high p_t region that is dominated by jet physics, the R_{AA} has been measured to be substantially less than 1 in central collisions at RHIC as well as at LHC, indicating a strong jet energy loss in the hot, color-opaque medium. With both RHIC and LHC R_{AA} measurements available now, there has been a lot of interest recently in quantifying the evolution of medium opaqueness with collision beam energy, and a few model studies indicate a sizable reduction of the opaqueness from RHIC to LHC [2–4].

A very important aspect of jet quenching study is the azimuthal anisotropy in the high p_t hadron production, which can be quantified by the azimuthal angle ϕ dependent nuclear modification factor $R_{AA}(\phi)$ [5–13]. Such anisotropy originates from the geometric features of the underlying matter distribution as well as the distribution of initial hard scattering spots. In off-central AA collisions, the overlap zone has an almond-like geometry in the transverse plane, which is then inherited by the created medium at early time. As a result, the jets with different transverse orientations (at mid-rapidity) would see different medium “thickness” and lose different amounts of energy, which leads to the azimuthal anisotropy in the distribution of final-state high p_t hadrons. The dominant component of this anisotropy is the second harmonic (often called the elliptic component) in the Fourier decomposition of $R_{AA}(\phi) \sim 1 + \nu_2^h \cos[2(\phi - \psi^{\text{EP}})]$. This ν_2^h should be differentiated from the commonly known elliptical flow ν_2^s of the soft hadrons, because of their distinctive origins: the former is from jet quenching while the latter is from the bulk medium’s collective expansion. At RHIC, most model calculations predicted a ν_2^h that is much smaller than the measured data. A first resolution of such discrepancy was proposed in Ref. [14] (referred to as the NTcE model hereafter) with a radical insight that the jet-medium interaction bears a nontrivial dependence on matter density and is strongly enhanced in the near- T_c matter via a non-perturbative mechanism, as motivated by the “magnetic scenario” for sQGP [15, 16]. The NTcE model successfully described the R_{AA} and ν_2^h as well as their centrality dependence at RHIC.

More recently it has been realized that anisotropy arises not only from the (average) geometric shape but also from strong fluctuations in the initial condition [17]. The aforementioned almond-shape picture for ν_2^h and ν_2^s assumes an averaged smooth geometry for the medium. The reality, however, turns out to be more complicated and interesting: event by event, the nucleon positions in the two colliding nuclei fluctuate, leading to the so-called initial state fluctuation (ISF), i.e., the fluctuation of the medium’s initial (entropy and energy) density distributions, which therefore bears different anisotropy in each event and leaves imprints in many observables. Detailed investigations over the past few years have revealed

that such initial state fluctuations are quite strong, and in fact even in perfectly central collisions the final hadron distribution shows nontrivial anisotropy. For example in the bulk matter evolution, such event-by-event anisotropy is translated by hydrodynamic expansion into different harmonic flows in the finally observed soft-hadron production. These have been observed in the RHIC and LHC experiments [18–22] and also demonstrated in various hydrodynamic calculations [17, 23–36]. It has also been shown that the so-called “soft ridge” — a strong peak on the near side in azimuthal angle and extending long in rapidity in the dihadron correlation — can be explained by convoluting such harmonic flow components in the single hadron distributions; see, e.g., [17, 24, 27, 32, 34, 37].

Since studies of the soft hadron distributions show convincing evidence for strong initial state fluctuations and event-by-event anisotropy beyond average geometry, and since the jet energy loss is a sensitive tomographic tool for anisotropy, one is naturally led to the questions of how such event-by-event anisotropy can be manifested in jet quenching observables such as the $R_{AA}(\phi)$ and what we can learn about jet energy loss from such observables. These are the central issues we aim to address, at least partially, in this study. Following the same argument about ν_2^h induced by the almond-like average geometry, one expects event-by-event azimuthal anisotropy for the high p_t hadrons can also arise from the fluctuating geometric distributions of *both the soft matter density and the initial jet-spot profile (the binary collision density)*. Some earlier discussions and data from RHIC and LHC can be found in Refs. [11, 19, 38–43]. In Ref. [5] we made the first attempt to study the connection between ISF and the jet azimuthal anisotropy (ν_n^h) and quantify the high p_t harmonics as the hard-probe response to the ISF, for the central collisions at RHIC with the fluctuations implemented via cumulant expansions. In the present paper we will present a systematic quantification, with full details and on an even-by-event basis, of how the hard probe responds to the geometry and fluctuations of the hot QCD matter created in heavy ion collisions from RHIC to LHC, substantiating previous studies reported in [2, 5, 14, 44]. We emphasize that this is an important shift for jet quenching physics, i.e., from studying an average anisotropy pattern $R_{AA}(\phi) \sim 1 + \nu_2^h \cos[2(\phi - \psi^{\text{EP}})]$ toward the event-by-event extraction of full anisotropy information $R_{AA}(\phi) \sim 1 + \sum_{n=1,2,3,\dots} \nu_n^h \cos[n(\phi - \psi_n^J)]$. In particular as alluded above, we want to gain a coherent picture about the jet quenching and its azimuthal anisotropy from RHIC to LHC, which is already partially investigated in Ref. [44]. The hope here is that by using geometric data at both collision energies, a strong constraint can be put on different jet quenching models, especially on how the energy loss depends on the path length and the medium density (temperature). In addition, understanding the jet-response anisotropy provides a sensitive tool for probing the initial conditions, which is complimentary to what can be learned from studying the bulk expansion responses. The analysis in the present paper will further address a number of important questions, including the event-by-event determinations of eccentricities ϵ_n and participant angles ψ_n in both RHIC and LHC experiments; the jet azimuthal anisotropy in terms of harmonics arising from geometry and fluctuations; comparison of these jet-response harmonics in different jet-energy-loss models; the transfer of eccentricities to jet-response harmonics and the angular correlations between ψ_n^J and ψ_n ; examination of the separate contributions to the jet anisotropy from the initial jet-spot-profile fluctuation and from the medium-density-profile fluctuation; and the sensitivity of the jet-response anisotropy to the composition of the matter density (in terms of participant and collision profiles).

In addition we will also study the azimuthal correlation between hard and soft hadrons [45, 46] (hard-soft correlation), much in parallel to the study of dihadron correlation in the

kinematic region dominated by soft hadrons. In particular we examine the contribution from their common correlations to the fluctuating initial conditions, as also initiated in Ref. [5]. Our improved calculation confirms what we previously found for the central collisions at RHIC: the hard-soft correlation shows a strong peak at near side (“hard-ridge”) and double-hump structure on the away side due to the concurrent harmonics in both soft and hard particle azimuthal distributions. We think this is a possible explanation of the “hard-ridge” [47–50]. Recently, the STAR collaboration has extracted the trigger-azimuthal-angle dependence of the dihadron correlation [51–53]. In Ref. [24], the trigger-angle (relative to ψ^{EP}) and p_t dependence of all the harmonic components extracted from the dihadron correlation were studied based on the hydrodynamic calculations. This approach should be good when the associated hadron p_t is around 0.15 – 3 GeV and trigger p_t is around 3 – 4 GeV). However for even higher p_t trigger (e.g., 4 – 6 GeV), the picture should be different because the jets become the dominant source and the correlation is of the hard-soft type. This hard-soft correlation will be studied based on our computation of jet response to ISF. We will also rederive the formula for the triggered correlation [54] by lifting the often used (and not fully correct) assumption that different event-plane angles ψ_n^J (for hard hadron) and ψ_n^S (for soft hadron) are totally correlated with ψ^{EP} (i.e., ψ_2^S).

Before getting into the main body of this study, we would like to emphasize two important discussions on the near- T_c enhancement model for jet quenching, which have been included as Appendices C and D. The first issue is about the possible relation between the strong near- T_c peak seen in the QCD trace anomaly (a measure of nonconformal behavior) and the proposed near- T_c enhancement in jet quenching, which arose during a discussion [55][56]. In Appendix C we will show that indeed the two phenomena could be simultaneously and consistently understood from the scenario of a near- T_c plasma of magnetic monopoles. The second issue concerns a quantitative estimate of the evolution of medium opacity from RHIC to LHC. The NTcE model with strong near- T_c enhancement of jet-medium interaction naturally predicts a less opaque medium at LHC, as the RHIC fireball has a larger fraction of its space-time evolution in the near- T_c region. In Appendix D, this is quantified to be a reduction of about 30% for the average jet-medium interaction, i.e., $\langle \kappa \rangle_{\text{RHIC}} : \langle \kappa \rangle_{\text{LHC}} \approx 1 : 0.72$ —consistent with a number of recent jet quenching analyses [3, 4, 57–59]. These are two important points and we choose to leave them in the Appendices primarily because they are somewhat less attached to the stream of main discussions in this paper.

The rest of the paper is organized as follows. In Sec. II, we collect the details of our Monte Carlo (MC) simulation. The initial state is modeled by using the MC Glauber model. Three different geometric jet-energy-loss models are presented. The structure of the simulation code can be found in Appendix A. Sec. III summarizes our results for the jet anisotropy at RHIC and LHC, and the comparison of different models. In Sec. IV, we discuss the (un)triggered hard-soft correlations. The re-derived formula for the triggered dihadron correlation can be found in Appendix B. A summary and some discussions will be given in Sec. V.

II. MC SIMULATION

In this section, we discuss the details of the MC simulation. The structure of the code can be found in Appendix A.

	ρ_0 (fm ⁻³)	R_A (fm)	d_A (fm)	\sqrt{B} (fm)	σ_{inel} (fm ²)	S_0 (fm ⁻³)	n
RHIC (0.2 TeV)	0.170	6.42	0.45	0.544	4.2	116	8.1
LHC (2.76 TeV)	0.166	6.67	0.44	0.660	6.2	291	6.0
LHC (5.50 TeV)	0.166	6.67	0.44	0.680	6.6	364	5.4

TABLE I: Parameters in the simulations for both RHIC and LHC. The explanation and the references for them can be found in the text.

A. Glauber model

In the AA collisions event by event, the positions of the nucleons fluctuate, as the result of the “measurement” of their positions (in the quantum language). This leads to the fluctuation of matter density, i.e., ISF. In the simulation, it is realized in a simplified way: sampling every nucleon position in the nuclei according to its density as measured in the low-energy scattering process [60]. The short range correlation between nucleons is included via requiring a smallest distance between them, which is set to 0.4 fm in most simulations (e.g., [29, 60]) including this work. The Glauber model is applied to deal with multiple NN collisions [60]: binary collision happens only if the transverse distance between two nucleons is smaller than $\sqrt{\sigma_{\text{inel}}/\pi}$. Here σ_{inel} is the total inelastic NN scattering cross section at the corresponding center of mass energy. The trajectory of each nucleon is always along the beam direction. The parameters in the simulation of the initial state are summarized in the following. First, the density in each colliding nuclei is parameterized in terms of the Wood-Saxon form [61]:

$$\rho(\mathbf{r}) = \frac{\rho_0}{\exp\left[\frac{(r-R_A)}{d_A}\right] + 1} . \quad (1)$$

The values of ρ_0 , R_A , and d_A for Au and Pb nuclei as used in RHIC and LHC can be found in Table I [61–63]¹. For the density in a nucleon, a Gaussian distribution is assumed in the transverse plane [61]:

$$T_p(\mathbf{r}^\perp) = \frac{\exp\left(-\frac{|\mathbf{r}^\perp|^2}{2B}\right)}{2\pi B} , \quad (2)$$

where the B value can be found in Table I for three different energies. Second, the total cross sections σ_{inel} for NN collisions at these energies are also listed in Table I. After the binary collisions are sampled by using the Glauber model based on σ_{inel} , we sum up contributions of all the “wounded” nucleons to get the participant density in the transverse plane:

$$\rho_p(\mathbf{r}^\perp) = \sum_{i=1}^{N_p} T_p(|\mathbf{r}^\perp - \mathbf{r}_i^\perp|) . \quad (3)$$

Here N_p is the number of wounded nucleons. A similar procedure can be applied to calculate the collision density $\rho_c(\mathbf{r}^\perp)$.

¹ The finite size of nucleons is taken into account when fixing the parameters in $\rho(\mathbf{r})$ as the sampling probability.

To make a connection between the initial state and the state of equilibrated medium, we assume that the entropy density S at $\tau \equiv \tau_0 = 0.6 \text{ fm}/c$ (around the equilibration time) is proportional to ρ_p at RHIC (0.2 TeV) [2, 5, 14], and a two-component profile, $(1 - \delta) \times \rho_p/2 + \delta \times \rho_c$, at LHC ($\delta = 0.118$ for both 2.76 and 5.5 TeV) [30, 62, 63]. The maximum entropy density in the central collisions, S_0 , is listed in Table I for different experiments [30, 63, 64], which are calibrated to the observed multiplicities in the hydrodynamic calculation. Based on this, we compute the proportionality coefficient in the relation between ρ_p and ρ_c , and $S(\tau_0)$. Before τ_0 , we assume effectively for jet quenching, the entropy density S grows linearly with time, while after that, the longitudinal expansion is applied and S decreases as $1/\tau$. See Ref. [38] for a detailed discussion about the effects of different preequilibrium models on jet quenching. Unfortunately, the medium's transverse dynamics is simplified without its hydrodynamical evolution, i.e., the shape is frozen, which will be discussed later. For the jets, their productions at the early stage of the collision should distribute according to ρ_c and are isotropic in their momentum space. In our simulation for each event, we integrate over all jet spots weighted by the binary collisional density from the same event, which is equivalent to using a large number of jets in each event. In the following section, we focus on the jet energy loss when traveling through the medium.

B. Jet quenching models

Three different geometric models are applied to compute the jet energy loss, which have distinctive geometric features (e.g., the path-length dependence) and matter-density dependence that are most crucial for describing geometric data [2, 5, 8, 10, 14, 38, 39]. Suppose the jet is produced with initial energy E_i . After traveling a path \mathbf{P} in the medium, the ratio between its final energy E_f and the initial energy E_i , i.e., the suppression factor $f_{\mathbf{P}}$, is given by

$$f_{\mathbf{P}} = \exp \left\{ - \int_{\mathbf{P}} \kappa[s(l)] s(l) l^m dl \right\} . \quad (4)$$

In this expression the $s(l)$ is the local entropy density at a given point on the jet path, and the $\kappa(s)$ is the local jet quenching strength which as a property of matter should in principle depend on the local density $s(l)$. There can be different choices of the parameter m for path-length dependence (e.g., LPM-motivated quadratic or AdS/CFT-motivated cubic) and of the jet-medium interaction $\kappa(s)$. In this study, we compare the following models [2, 14]: the near- T_c enhancement (NTcE) model, L^2 model, and L^3 model. The NTcE model assumes $m = 1$ and introduces a strong jet quenching component in the vicinity of T_c (with density s_c and span of s_w) via

$$\kappa(s) = \kappa_0 [1 + \xi \exp(-(s - s_c)^2/s_w^2)] , \quad (5)$$

with $\xi = 6$, $s_c = 7/fm^3$, and $s_w = 2/fm^3$. (see [14] for details.) In the L^2 (L^3) model, $\kappa(s) = \kappa_0$ is constant and $m = 1$ ($m = 2$). In each model, the parameter κ_0 will be fixed by $R_{AA} \approx 0.18$ in the 0 – 5% collisions at RHIC $\sqrt{s} = 0.2 \text{ TeV}$, and then will be applied at LHC $\sqrt{s} = 2.76, 5.5 \text{ TeV}$.

To calculate the azimuthal angle dependence of the nuclear modification factor, we can apply the following formula:

$$R_{AA}(\phi) = \langle (f_{\mathbf{P}})^{n-2} \rangle_{\mathbf{P}(\phi)} . \quad (6)$$

A detailed derivation of Eq. (6) can be found in Ref. [65].² Here $\langle \dots \rangle_{\mathcal{P}(\phi)}$ means averaging over all jet paths with the propagation orientation fixed at angle ϕ relative to the reaction plane, including all the possible initial jet production points [distributed according to $\rho_c(\mathbf{r}^\perp)$]. The exponent n is the spectrum index of the measured high p_t spectrum in a reference p-p collision. It should be emphasized here that the index n depends on the p-p collision energy. In Table I, we show n at the three different energies [65–67]. To calculate the over all modification factors, R_{AA} , we need to average over all the jet paths with different orientation angles that are equally distributed.

Moreover, in these models, assuming the fractional energy loss leads to $R_{AA}(\phi)$ being independent of p_t . This at RHIC energy may be justified by the approximate “flatness” seen in the R_{AA} vs p_t data. At LHC energies, we expect the p_t dependence of the azimuthal anisotropy, i.e., $R_{AA}(\phi)/R_{AA}$, to be weak, which should be dictated by the length and density dependence of the jet energy loss in the transverse plane. The results from such modeling apply only to the high- p_t region, e.g., $p_t > 6$ GeV at RHIC 0.2 TeV, and $p_t > 8$ GeV at LHC 2.76 TeV.³

In the simulation of each event, we apply the Fourier-decomposition to $R_{AA}(\phi)/R_{AA}$:

$$R_{AA}(\phi) = R_{AA} \left(1 + 2 \sum_n \nu_n^h \cos[n(\phi - \psi_n^J)] \right). \quad (7)$$

In each event the azimuthal anisotropy can be represented by the collection of ν_n^h and ψ_n^J . The importance of different harmonics decreases with increasing n except for the second harmonics, as will be shown later. So we focus on the first six harmonics in this work.

III. THE ISF AND JET AZIMUTHAL ANISOTROPY

A. The ISF

To quantify the ISF in each AA collision, the following eccentricities ϵ_n are defined, as motivated by the cumulant expansion method in Ref. [28]:

$$\epsilon_{n \geq 2} \equiv - \frac{\langle r^n \cos[n(\phi - \psi_n)] \rangle}{\langle r^n \rangle}, \quad (8)$$

$$\psi_{n \geq 2} = \frac{1}{n} \arctan \left(\frac{\langle r^n \sin(n\phi) \rangle}{\langle r^n \cos(n\phi) \rangle} \right) + \frac{\pi}{n}, \quad (9)$$

$$\epsilon_1 \equiv - \frac{\langle r^3 \cos[(\phi - \psi_1)] \rangle}{\langle r^3 \rangle}, \quad (10)$$

$$\psi_1 = \arctan \left(\frac{\langle r^3 \sin(\phi) \rangle}{\langle r^3 \cos(\phi) \rangle} \right) + \pi. \quad (11)$$

The ψ_n is the reaction plane angle of n th harmonics. $\langle \dots \rangle$ means averaging over the entropy density at τ_0 .

² This formula shows that the quenching effect increases when the overall jet energy loss increases. Meanwhile, for a given energy loss fraction, a softer p-p collision spectrum (i.e., with a larger n) leads to a larger quenching.

³ At LHC 5.5 TeV, the threshold maybe somewhat higher.

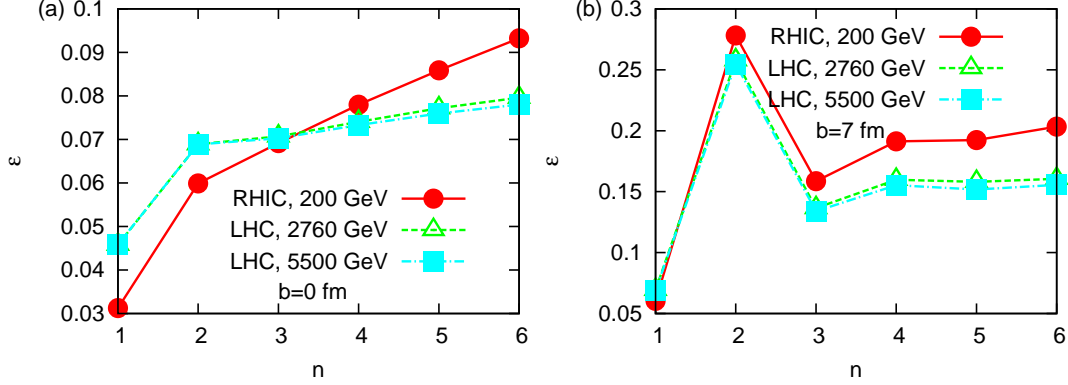


FIG. 1: (Color online). The spectrum of ϵ_n at $b = 0, 7$ fm for RHIC with $\sqrt{s} = 200$ GeV and for LHC with $\sqrt{s} = 2760, 5500$ GeV.

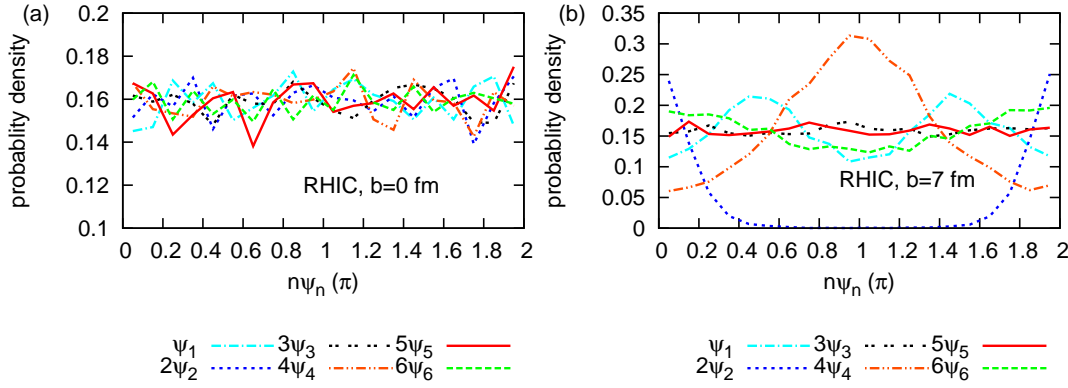


FIG. 2: (Color online). The distribution of ψ_n for $b = 0, 7$ fm at RHIC ($\sqrt{s} = 200$ GeV). For $b = 7$ fm, $(2\psi_2)$'s probability density is scaled down by a factor 0.3. Similar results for LHC ($\sqrt{s} = 2760, 5500$ GeV) can be found in Figure 15.

Figure 1 shows the ϵ_n spectrum for $b = 0$ fm (most central collision) and $b = 7$ fm (peripheral collision) at three different collision energies. For all the experiments, in the central collisions, ϵ_n are close while in the peripheral collisions, ϵ_2 dominates due to the almond-like geometry. Moreover, ϵ_n at LHC 2.76 TeV and LHC 5.5 TeV are almost the same. In Figs. 2 and 15, we plot the distributions of ψ_n relative to the reaction plane for $b = 0$ and 7 fm in three cases [28]: in the central collisions, ψ_n do not have specific orientation; in the peripheral collisions, ψ_1 and ψ_4 tend to lie in the $\pi/2$ and $\pi/4$ directions; ψ_2 is strongly correlated with the reaction plane (in the plot, ψ_2 's probability density is scaled down by a factor 0.3); other odd ψ_n distribute randomly. We also check that the correlation between any two angles vanishes in the central collisions. Figs. 3 and 16 list the b dependence of the eccentricities, which shows the similarity in three experiments and also the emergence of the second harmonic dominance in the peripheral collisions. In addition, Figure 4 shows the relations between N_p (N_c) and b . The error bars indicate their r.m.s values, which are small except in the very peripheral collisions. In the following, we will show the results against b . Figure 4 can be used to compute the corresponding N_p dependence.

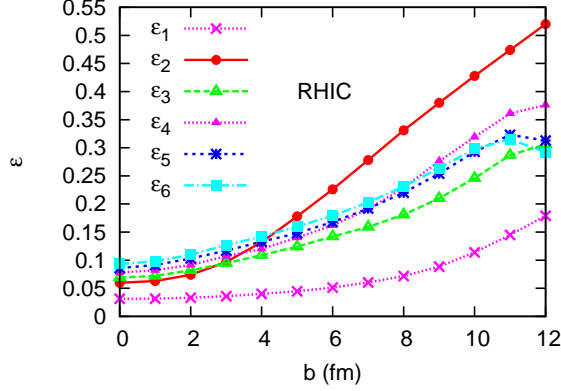


FIG. 3: (Color online). The b dependence of ϵ_n for RHIC ($\sqrt{s} = 200$ GeV). Similar results for LHC ($\sqrt{s} = 2760, 5500$ GeV) can be found in Figure 16.

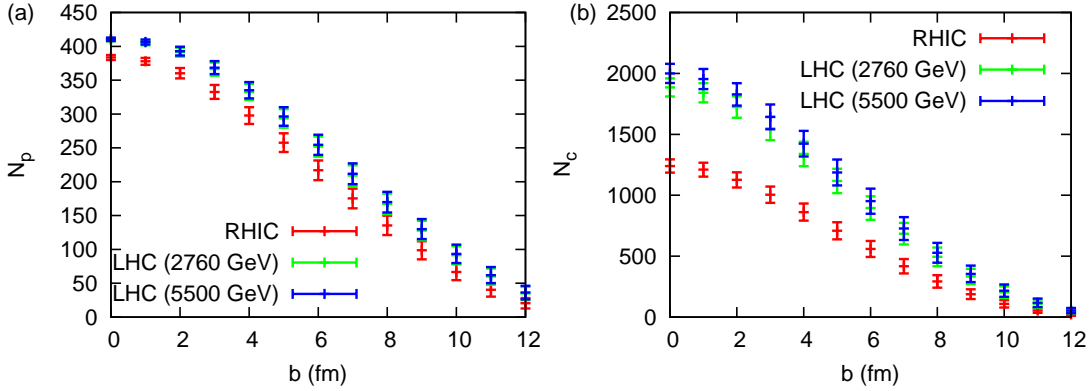


FIG. 4: (Color online). The b dependence of N_p and N_c for both RHIC ($\sqrt{s} = 200$ GeV) and LHC ($\sqrt{s} = 2760, 5500$ GeV).

B. The jet azimuthal anisotropy

In this section, we focus on results for the jet azimuthal anisotropy. Figs. 5 and 17 show the ν_n^h spectrum [see Eq. (7)] in both most central collision ($b = 0$ fm) and peripheral collision ($b = 7$ fm) as calculated by using different jet energy loss models. We can see that the second harmonics dominate in the peripheral collision reflecting the almond-like geometry in the peripheral collisions, and other harmonics decrease with increasing n in both central and peripheral collisions. More importantly, for the first three harmonics, the NTcE and L^3 result for RHIC (0.2 TeV) are close, while for LHC (2.76, 5.5 TeV) the NTcE and L^2 result are close. The b dependence of ν_n^h in the three experiments as predicted by the models is shown in Figs. 6, 7, and 18 (curves labeled as “model ν ”). $\langle \cos[n(\psi_n^J - \psi_n)] \rangle$, which reflects the correlation between ψ_n^J and ψ_n [68], is also plotted in these figures against different b for different harmonics (curves labeled as “model c ”). As illustrations, Figs. 19, 20, and 21, at the end of this article, show the distribution of $\psi_n^J - \psi_n$ computed by using different models for $b = 0$ and 7 fm in the three experiments. Interestingly, the authors in Ref. [29] presented similar distribution of $\psi_n^S - \psi_n$ [Here ψ_n^S is the angle of n th harmonic event plane reconstructed from the final low p_t hadron azimuthal distribution; see Eq. (B1)]. By comparing the two, we find that for the second and third harmonics, ψ_n^J and ψ_n^S have

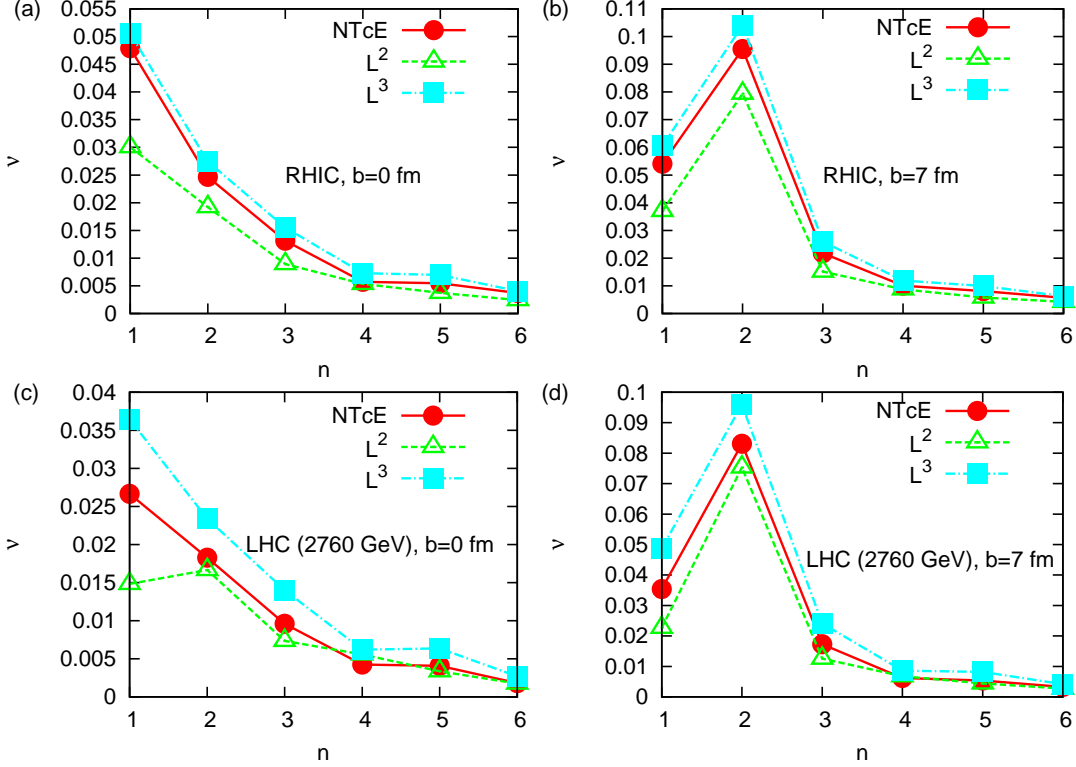


FIG. 5: (Color online). The spectrum of ν_n^h for RHIC ($\sqrt{s} = 200$ GeV) and LHC ($\sqrt{s} = 2760$ GeV) at $b = 0, 7$ fm, based on three different models. Similar results for LHC ($\sqrt{s} = 5500$ GeV) can be found in Figure 17.

similar distribution relative to the ψ_n , although ψ_n^J distributions computed by three models differ somewhat; for the other higher harmonics, ψ_n^J and ψ_n^S gains much broader distribution relative to ψ_n , and $\langle \cos[n(\psi_n^J - \psi_n)] \rangle$ changes from positive to negative with decreasing b (the value of the transition b depends on individual jet energy loss model). On the other hand, the experimental measurement of ν_n^h is normally not the ν_n^h shown in Figs. 6, 7, and 18, but its projection to ψ_n^S , i.e., $\langle \nu_n^h \cos[n(\psi_n^J - \psi_n^S)] \rangle$.⁴ Because of missing soft dynamics in our simulation, we can not calculate $\langle \cos[n(\psi_n^J - \psi_n^S)] \rangle$ at this stage. However, for the second harmonics ν_2^h , based on the $\langle \cos[2(\psi_2^J - \psi_2)] \rangle$ shown here and the $\psi_2^S - \psi_2$ distribution shown in Ref. [29], the effect of this angle dispersion should be less than 5% reduction for peripheral collision ($b \geq 6$ fm). This provides solid ground for comparing the data for ν_2^h with our results to differentiate different jet energy loss models, as carried out in [44]. There it was found that the RHIC ν_2^h data favor the NTcE and L^3 models, while the LHC (2.76 TeV) ν_2^h data favor the NTcE and L^2 models. This is consistent with ν_2^h shown in Figs. 6, 7, and 18. Meanwhile, ν_1^h and ν_3^h deliver valuable information about the orders of magnitude of the measured harmonics, although the angle dispersion can bring substantial reduction yet without changing the sign. It is conceivable that the experimental data on ν_n^h will bring important constraints to the jet quenching models. A tentative try along this direction is pursued in Ref. [44].

⁴ The other measurement of ν_n^h is to project the ν_n^h to the second harmonic event plane, i.e., $\langle \nu_n^h \cos[n(\psi_n^J - \psi_2^S)] \rangle$.

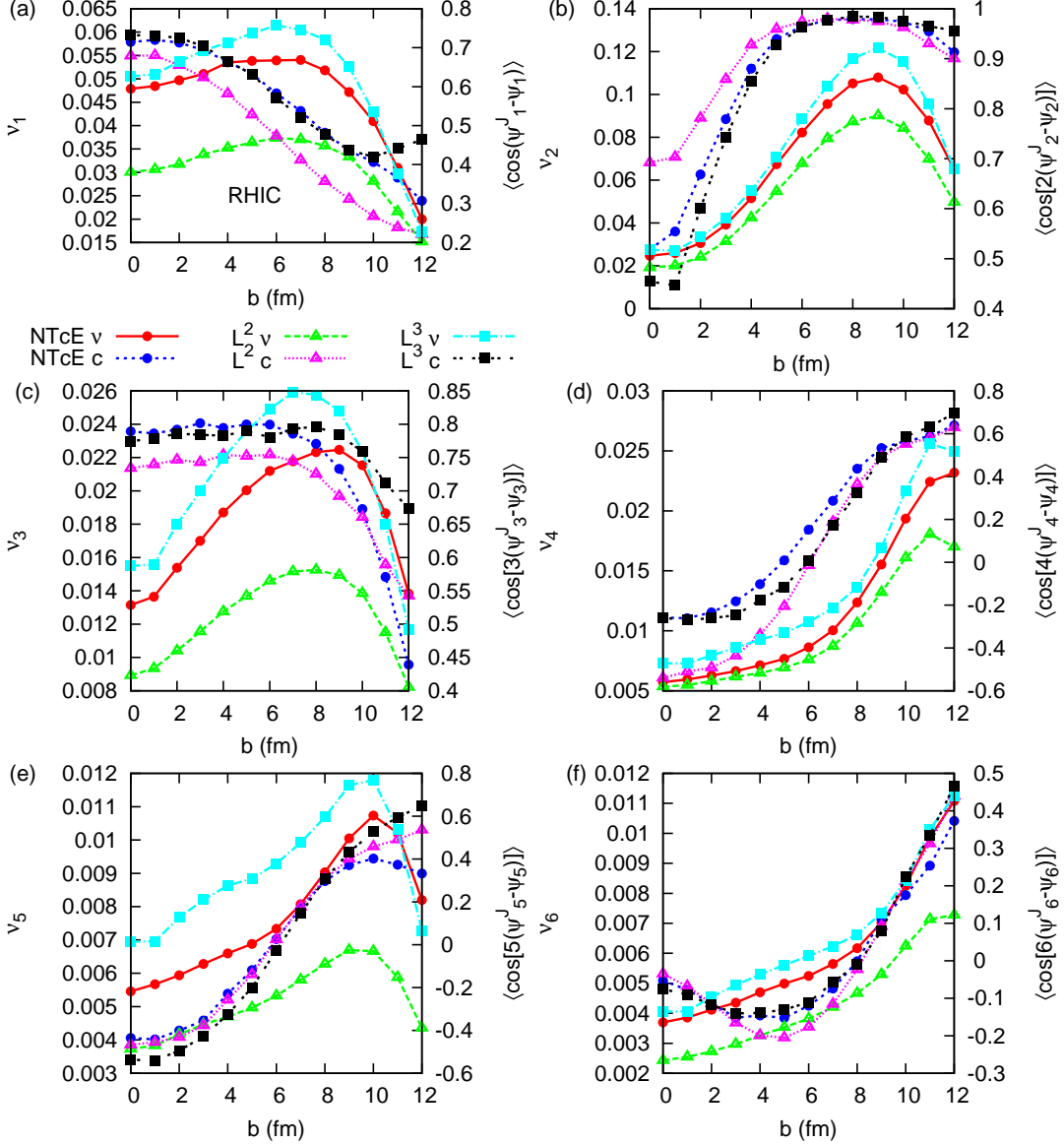


FIG. 6: (Color online). The b dependence of ν_n^h and $\langle \cos[n(\psi_n^J - \psi_n)] \rangle$ for RHIC ($\sqrt{s} = 200$ GeV) based on three different models.

Let us also take a look at the correlation between ψ_n^J and the participant plane ψ_2 . For the central collisions, we can expect ψ_n^J to distribute randomly with respect to ψ_2 , which is confirmed by our simulation results for RHIC (0.2 TeV). However, in the peripheral collisions, things become tricky. Figure 8 shows the $\psi_n - \psi_2$ and $\psi_n^J - \psi_2$ distributions at RHIC (0.2 TeV) with $b = 7$ fm.⁵ For the ISF eccentricities, $\psi_1 - \psi_2$ and $\psi_4 - \psi_2$ are mostly around $\pi/2$ and $\pi/4$, while ψ_3 distribute randomly. The $\psi_n^J - \psi_2$ distribution (in Figure 8) seems consistent with the combined information about $\psi_n - \psi_2$ distribution (in Figure 8) and $\psi_n^J - \psi_n$ distribution (in Figure 19) except for the 1st harmonics. From $\psi_1^J - \psi_1$ and

⁵ The $\psi_2 - \psi_2$ distribution in principle should be a delta function. The plot (b) of Figure 8 serves as a confirmation of our numerics.

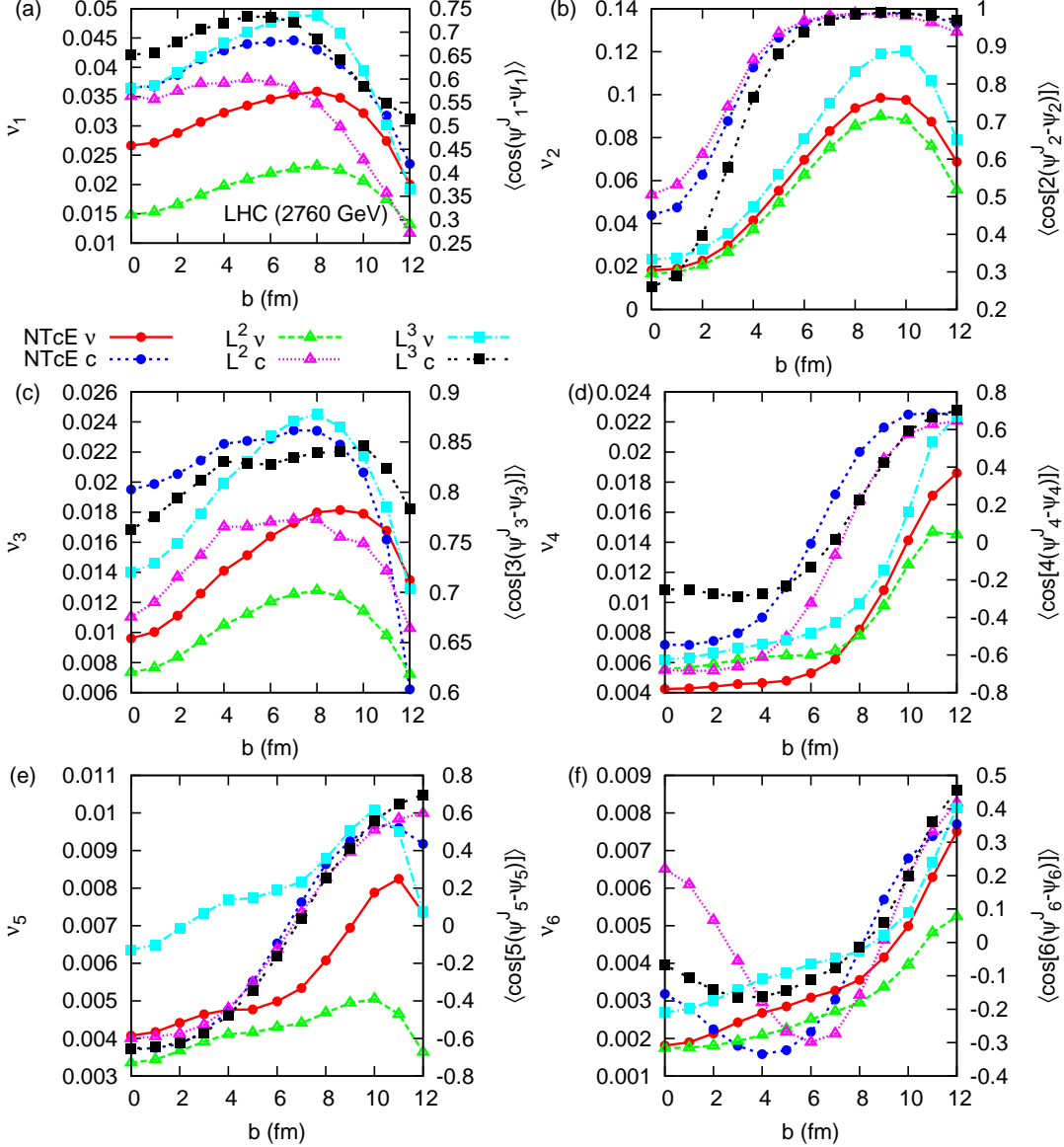


FIG. 7: (Color online). The b dependence of ν_n^h and $\langle \cos[n(\psi_n^J - \psi_n)] \rangle$ for LHC ($\sqrt{s} = 2760$ GeV) based on three different models.

$\psi_1 - \psi_2$ distribution, we expect $\psi_1^J - \psi_2$ to be around $\pi/2$, but Figure 8 shows $\psi_1^J - \psi_2$ to be around 0. This problem is resolved by noticing that the $\psi_1^J - \psi_1$ distribution is broader when $\psi_1 - \psi_2$ is around $\pi/2$ compared to when $\psi_1 - \psi_2$ is around 0. Furthermore it implies the conventional picture that ψ_1^J (or ψ_1^S) randomly distributes is flawed.

It is also interesting to separate the contribution to ν_n^h from jet spot (JS) fluctuation and from the matter density fluctuation. Figure 9 shows the ν_n^h due to the full fluctuation (i.e., total response) and only due to the jet spot fluctuation (i.e., JS response) in the central collision at RHIC and LHC (2.76 TeV) by using the NTcE model. Here the JS response is computed by removing the fluctuations in the matter density. We can see that, for the first three harmonics, the jet spot contribution is significant. The difference between total response and JS response can be considered as the response due to the matter density fluctuation (i.e., MD response). To compute the difference, we need information about

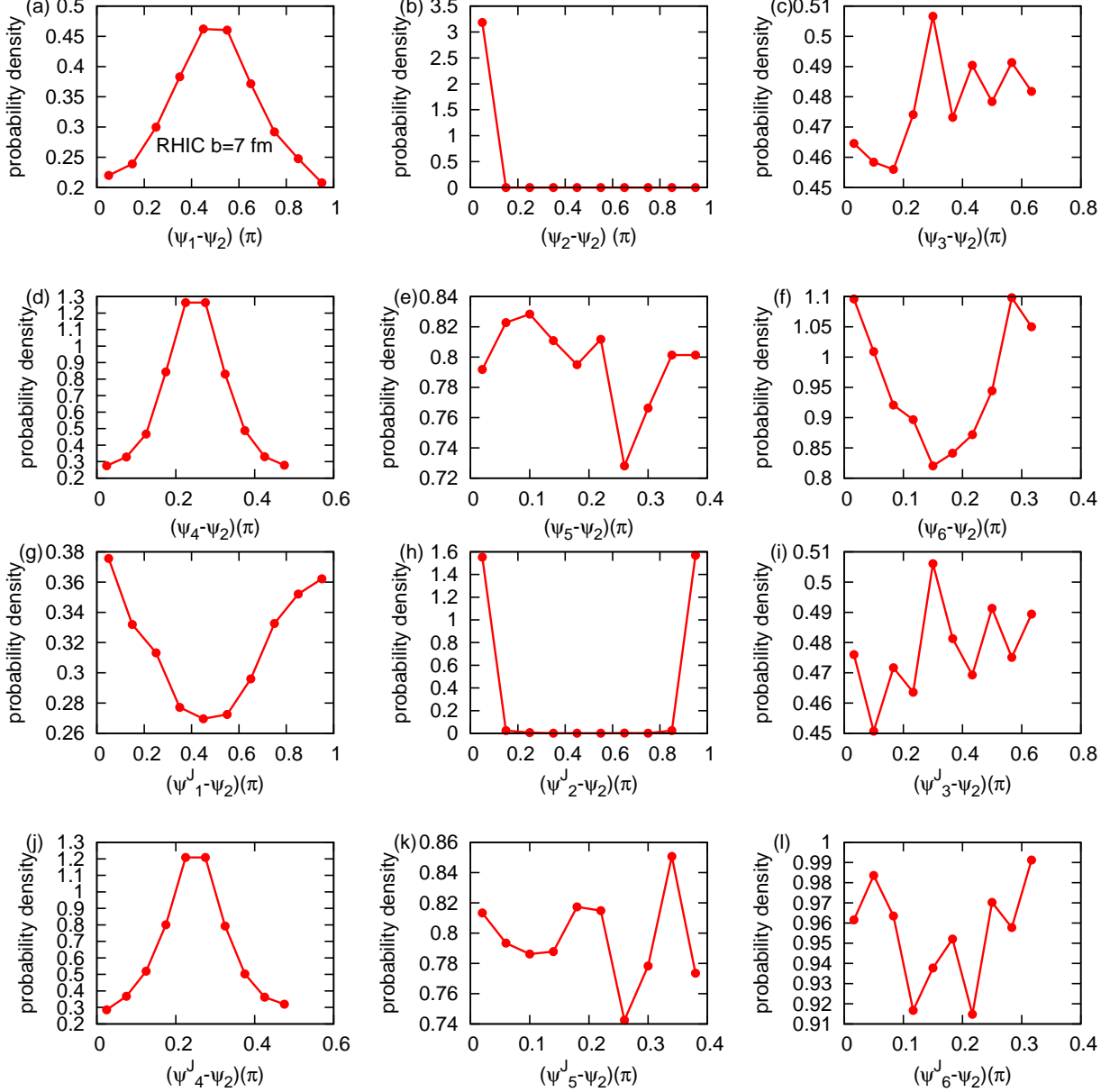


FIG. 8: (Color online). The distribution of $\psi_n - \psi_2$ and $\psi_n^J - \psi_2$ for RHIC ($\sqrt{s} = 200$ GeV) calculated by using the NTcE model.

the sign of the responses as shown in Figure 10 which plots the corresponding $\psi_n^J - \psi_n$ distribution. The plots indicate that, for the first and third harmonics in both experiments, the total and JS response are positive, but in the second harmonics, the total response is positive and the JS response is negative. Combining the information about ν_n^h with the $\psi_n^J - \psi_n$ distribution, we find that, for the first harmonics, the total response is dominated by the JS response while the MD response plays a cancellation role; for the second harmonics, the MD response is positive and the JS response plays a cancellation role; for the third harmonics, both MD and JS response are positive. For the other higher order harmonics, the JS response becomes less significant. The result is also consistent with our earlier simple estimate [5]. This shows that the jet anisotropy is a probe both the initial collision density profile at very early stage of AA collision and the matter density profile during

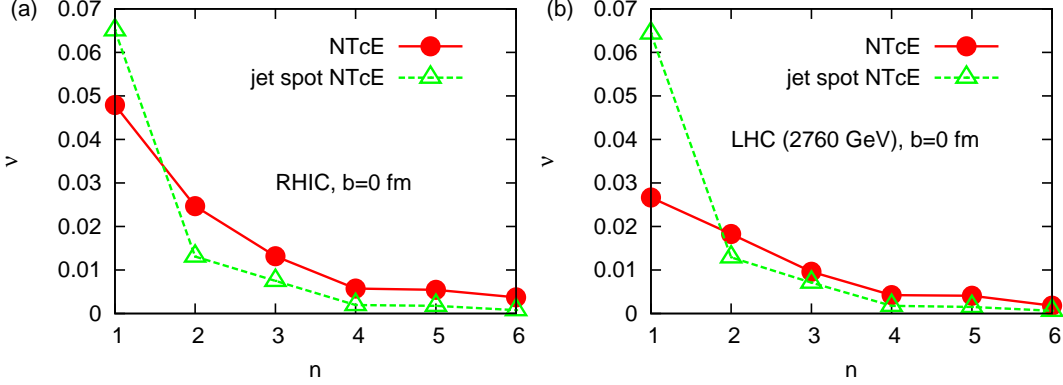


FIG. 9: (Color online). The spectrum of ν_n^h for both RHIC ($\sqrt{s} = 200$ GeV) and LHC ($\sqrt{s} = 2760$ GeV) central collisions due to full calculation of NTcE model (“NTcE” curve) and the contribution of the jet spot fluctuation in NTcE model (“jet spot NTcE” curve).

the jet traveling through the medium; different ν_n^h with the two playing different roles put important constraints on modeling both effects.

Furthermore, is the jet anisotropy sensitive to the composition of the entropy density? In Figure 11, we compare the results for LHC (2.76 TeV) based on two different media ($b = 0$ and 7 fm); the NTcE calculation is the same as the NTcE for LHC (2.76 TeV) in Figure 5 assuming the two-component profile, $S(\tau_0) \sim (1 - \delta) \times \rho_p/2 + \delta \times \rho_c$, but the “ ρ_p NTcE” assumes $S(\tau_0) \sim \rho_p$. This shows that the first three harmonics are sensitive to different entropy densities. Especially, ν_1^h with ρ_p density profile is 60% and 40% bigger than with the mixed profile at $b = 0$ and 7 fm. The $\psi_n^J - \psi_n$ distributions in the two cases, as we have checked, are quite close. Although the conventional procedure uses the multiplicity vs b to calibrate δ in the two-component entropy density, our results suggest studying jet anisotropy to be another way to constrain the density profile.

IV. HARD-SOFT CORRELATION

Motivated by the experimental analysis in Ref. [69], we study the (un)triggered azimuthal correlation between hard and soft hadrons at mid-rapidity. Following Refs. [54, 69], the triggered dihadron correlation is the pair distribution relative to angle difference, i.e., $\phi^h - \phi^s$, with ϕ^h constrained in specific region, \mathcal{R} . Here \mathcal{R} is composed of four different pieces: $\phi_\alpha - \phi_\beta \leq \phi^h - \psi^{\text{EP}} \leq \phi_\alpha + \phi_\beta$ (ϕ_α is in the first quadrant) and other three with $\phi_\alpha \rightarrow -\phi_\alpha, \pi + \phi_\alpha, \pi - \phi_\alpha$. In Appendix B, we derive necessary formula for the computation. Similar calculation has been done in Ref. [54], but we keep track the difference between ψ_n^S (ψ_n^J) and ψ_2^S (also called the event plane angle ψ^{EP}). To compute the untriggered correlation, we can simply set $\phi_\alpha = \phi_\beta = \pi/4$. Because the medium evolution in the transverse plane and the subsequent hadronization are not included in our simulation, we simply assume that (1) the event plane angle ψ^{EP} is the same as ψ_2 ; (2) $\nu_n^s = \chi_n^s \epsilon_n$ for the first four harmonics [5]⁶; and (3) perfect alignment between ψ_n^S and ψ_n . We set $\chi_{n=1,2,3,4,5}^s \approx 0.15, 0.26, 0.21, 0.14, 0.086$

⁶ Ref. [29] shows that $\nu_n^s \sim \epsilon_n$ is valid for the first three harmonics in general but only valid for the fourth in the central collisions.

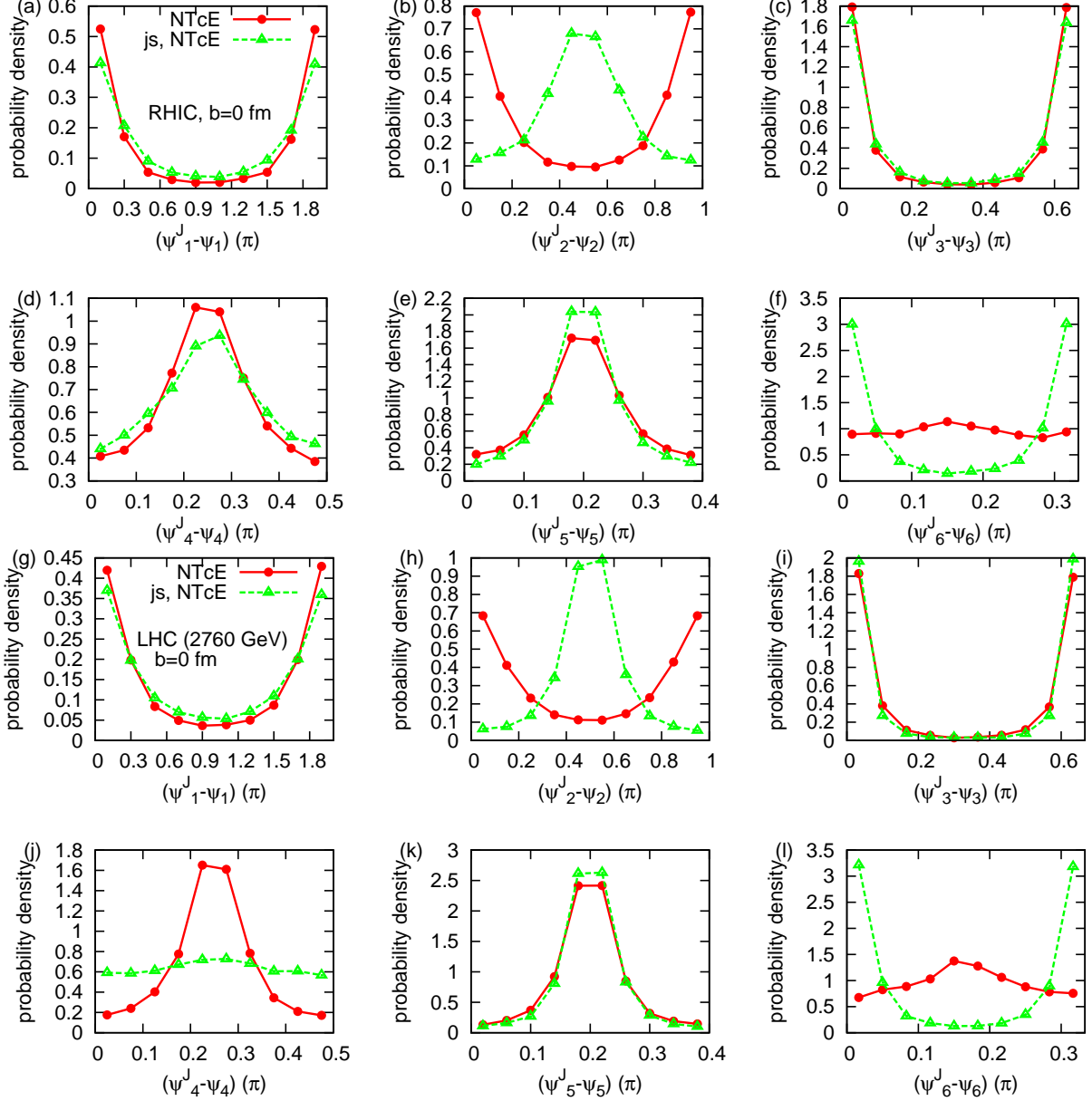


FIG. 10: (Color online). The distribution of $\psi_n^J - \psi_n$ for RHIC ($\sqrt{s} = 200$ GeV) and LHC ($\sqrt{s} = 2760$ GeV) due to full calculation of the NTcE model (“NTcE” curve) and the contribution of the jet spot fluctuation in the NTcE model (“js NTcE” curve).

respectively (see e.g., [23, 26, 28, 29]), which are for the associated hadrons with p_t around 2 – 4 GeV at RHIC (0.2 TeV).

In Ref. [5], we made a simple estimate of the untriggered dihadron correlation in the central collisions at RHIC (0.2 TeV). Here we can improve the previous calculation by simulating the realistic density profile and including the $\psi_n^J - \psi_n$ distribution ($\psi_n^J = \psi_n$ was assumed before). Let us apply the following decomposition:

$$C(\Delta\phi) \equiv 2 \times \left[\sum_n V_{n\Delta} \cos(n\Delta\phi) \right],$$

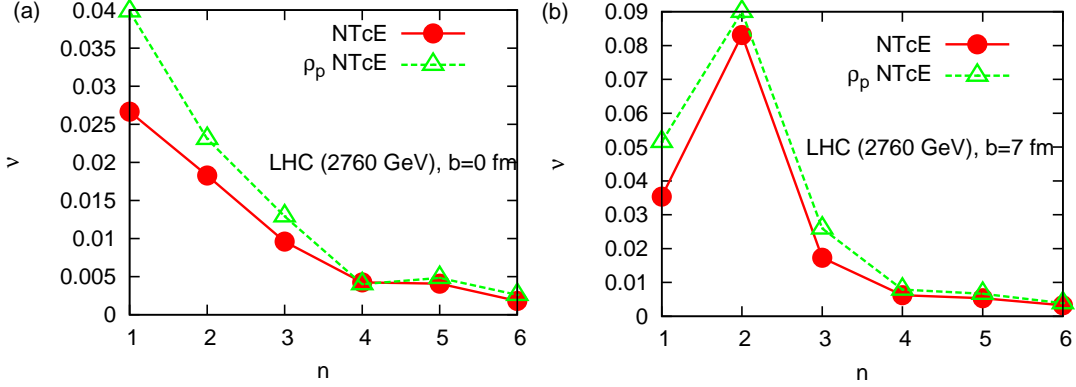


FIG. 11: (Color online). The spectrum of ν_n^h for LHC ($\sqrt{s} = 2760$ GeV) due to full calculation of the NTcE model (“NTcE” curve) and the same model with entropy density scaled with ρ_p (“ ρ_p NTcE” curve).

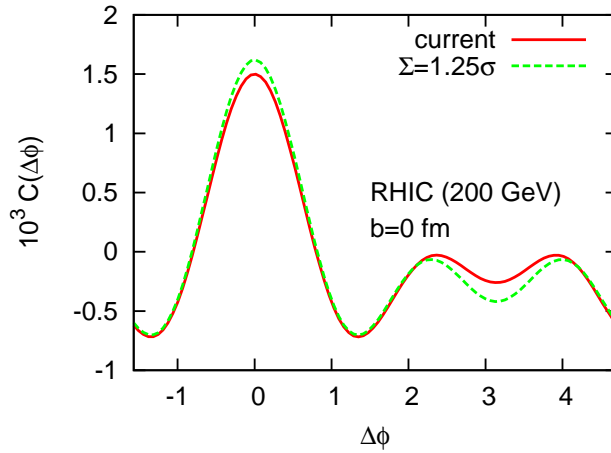


FIG. 12: (Color online). The untriggered dihadron correlation $C(\Delta\phi)$ in central collisions at RHIC ($\sqrt{s} = 200$ GeV) as calculated in our simulation (“current” curve) and our estimate (“ $\Sigma = 1.25\sigma$ ” curve) in Ref. [5]. The two calculations are all based on the NTcE model. $\Sigma = 1.25\sigma$ is a reasonable choice of a parameter in the previous estimate.

where the definition of $C(\Delta\phi)$ can be found in Appendix B. Here we collect the results of the current calculation (previous estimate)⁷: $V_{1\Delta} = 2.3 (2.8) \times 10^{-4}$, $V_{2\Delta} = 3.1 (3.0) \times 10^{-4}$, and $V_{3\Delta} = 2.1 (2.3) \times 10^{-4}$ (higher harmonics are at the 10% level of the first three). Both calculations are based on the same NTcE model. Figure 12 shows the comparison for $C(\Delta\phi)$. We can see that the structures of $C(\Delta\phi)$ are quite close.

In Figure 13 following Ref. [24], we show our results for $V_{n\Delta}$ ($n = 1, 2, 3$) vs trigger direction ϕ_α with $b = 7$ fm at RHIC (0.2 TeV) based on the NTcE model. The ϕ_β is set as $\pi/24$, as in Ref. [69]. The even harmonics $V_{2\Delta}$ and $V_{4\Delta}$ (not shown in the plot) are dominated by $\cos(2\Delta\psi_2^S)t_2$ and $\cos(4\Delta\psi_4^S)t_4$ [see Eq. (B4)], which lead to $\cos(2\phi_\alpha)$ and $\cos(4\phi_\alpha)$ dependence. The odd harmonics $V_{1\Delta}$ and $V_{3\Delta}$ are much smaller (in the plot, they

⁷ The results of the previous estimate, as shown here, are with parameter Σ set to 1.25σ . See Ref. [5] for details.

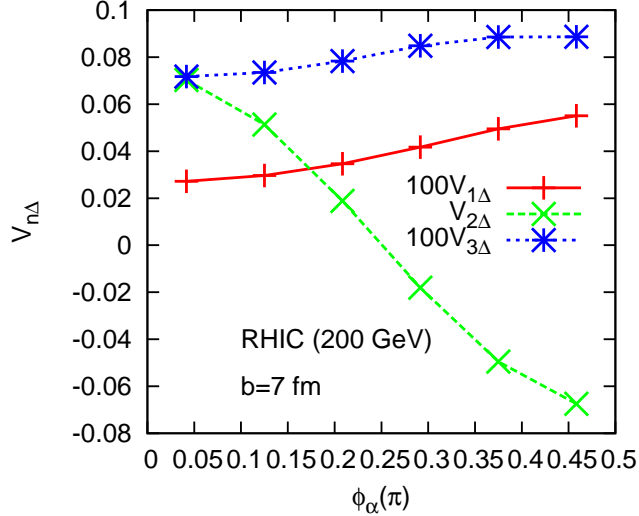


FIG. 13: (Color online). The triggered dihadron correlation $V_{n\Delta}$ vs trigger direction ϕ_α with $b = 7$ fm at RHIC ($\sqrt{s} = 200$ GeV). ϕ_β is set to $\pi/24$, following Ref. [69]. The calculation is based on the NTcE model.

are scaled up by a factor of 100). The $V_{1\Delta}$ has some ϕ_α dependence because of the mentioned nonuniform distributions of $\psi_1^J - \psi_2$ and $\psi_1 - \psi_2$ as shown in Figure 8, while $V_{3\Delta}$ depends much less weakly on ϕ_α . The author in Ref. [24] extracted $V_{n\Delta}$ directly from the unsubtracted correlation data in Ref. [69].⁸ Note our $V_{1\Delta}$ is positive, but $V_{1\Delta}$ of Ref. [24] is negative, which, however, is consistent with the result that ν_1^s of the associated hadron is negative when p_t is below 1 – 2 GeV, and positive when p_t becomes bigger. In addition, the extracted $V_{1\Delta}$ can have a contribution from the correlation due to momentum conservation, although a rapidity gap was required in the extraction. Our $V_{2\Delta}$ is similar to that in Ref. [24]. However, the overall sign of our estimated $V_{4\Delta}$ is opposite to the $V_{4\Delta}$ in Ref. [24], because we approximate $\cos(4\Delta\psi_4^S)$ in Eq. (B4) by $\cos[4(\psi_4 - \psi_2)]$. It turns out that, although $\psi_4 - \psi_2$ is around $\pi/4$ (see Figure 8), the hydrodynamic calculation shows for the final hadron spectrum $\psi_4^S - \psi_2$ is around 0 [29]. So we expect that, in the full calculation with medium evolution included, the sign of $V_{4\Delta}$ can be corrected (the magnitude could be changed because the linear response approximation fails in this case). Because $\tilde{\nu}_n^h$ has no p_t dependence in our calculation, the p_t dependence of $V_{n\Delta}$ is the same that of ν_n^s , which is consistent with the analysis of p_t dependence in Ref. [24].

V. SUMMARY

In summary, we have performed a systematic and event-by-event study of the jet azimuthal anisotropy for both $Au - Au$ collisions at RHIC ($\sqrt{s} = 0.2$ TeV) and $Pb - Pb$ collisions at LHC ($\sqrt{s} = 2.72$ and 5.5 TeV). The MC Glauber model is used to generate the initial state density profile that fluctuates strongly from event to event. Three different geometric jet-energy-loss models, including NTcE, L^2 , and L^3 that represent the characteristic

⁸ Although the trigger p_t is around 2 – 4 GeV in the extraction [24], it was mentioned that, for the higher p_t trigger, 4 – 6 GeV, the ϕ_α and associate p_t dependence of $V_{n\Delta}$ are similar to those with lower p_t trigger.

path-length and density dependence of the near-Tc enhancement, pQCD, and AdS/CFT models, are explored and compared at both RHIC and LHC (2.76 TeV). In each event, we extract ν_n^h , the high p_t event plane angles ψ_n^J and the initial participant plane angles ψ_n . For the second harmonics, we see ψ_2^J is strongly correlated with ψ_2 in peripheral collisions as predicted by all the models for different experiments. It is reasonable to assume a strong correlation between ψ_2^S and ψ_2 , as demonstrated by the hydrodynamic calculation (e.g., [29]). Based on this, we can directly compare the ν_2^h with the measured ν_2 of high p_t hadrons, as carried out in Ref. [44]. There it was found that the NTcE and L³ models can explain the high p_t ν_2 data at RHIC while the NTcE and L² models succeed in describing LHC (2.76 TeV) data. One therefore concludes that taking together the geometric data at both RHIC and LHC, only the NTcE model describes all data sets. In addition, as discussed in Appendix D in detail, the NTcE model naturally explains lower opaqueness of the medium created at LHC as compared with that at RHIC; i.e., a reduction of jet-medium interaction at $\sim 30\%$ level as also implied by data. We also analyze the correlation between ψ_n^J and ψ_n for other harmonics. For the first and third harmonics, $\langle \cos[n(\psi_n^J - \psi_n)] \rangle$ are around 0.6 – 0.8 except in very peripheral collisions, but for the fourth and higher harmonics, even the sign can change although the specific transition impact parameter depends on models and experiments. This seems consistent with the LHC (2.76 TeV) data shown in Ref. [44], which right now are not converging but do indicate negative responses for higher harmonics. We further clarify that, in the middle-central collisions (e.g., $b = 7$ fm) at RHIC, although ψ_3 and ψ_3^J do have a random distribution, the first harmonic turns out to be tricky: ψ_1 has slight preference in the out-of-plane direction but ψ_1^J prefers to be along the in-plane direction. For the fourth harmonics at $b = 7$ fm, both ψ_4 and ψ_4^J fluctuate around $\pi/4$ relative to either participant plane ψ_2 or the reaction plane. It is also interesting to separate the contributions to the jet anisotropy. In the central collisions at RHIC, we have analyzed the effect of the initial jet spot fluctuation. The difference between the JS response and the full response should be due to the matter density (shape) fluctuation. We see in the first three harmonics their roles are different, which points out the importance of having a coherent picture for all these harmonics in a valid model. We also test the sensitivity of the jet anisotropy to the composition of the matter density in the Glauber model, which shows at LHC (2.76 TeV) that the first three harmonics are affected significantly by changing the entropy density from a combination of participant and collision density to the participant density alone. Although the mixing of the two in the matter density is normally calibrated to the observed multiplicity vs b , our test does show another interesting way to calibrate this.

Based on the information about jet anisotropy and assuming that the response of the collective flow to ISF is linear, we proceed to discuss both untriggered and triggered hard-soft correlation. For the central collisions at RHIC, we have improved our calculation of the untriggered correlation in Ref. [5] and confirmed the results there: a strong peak develops on the near side (“hard ridge”) while a double-hump structure shows up on the away side. This could be a possible explanation for the experimentally observed “hard ridge”, but the away side structure can be more complicated because of the other sources of correlations (e.g., effects of global momentum conservation and cluster correlation [70, 71]), which requires more detailed study. By using our rederived formula for the triggered correlation, we have studied the Fourier component of the correlation, $V_{n\Delta}$. We find that the trigger-angle dependence of $V_{n\Delta}$ is consistent with the extracted information in Ref. [24]. As for the associated p_t dependence of the hard-soft correlation, we expect it to be the same as that of $\nu_n^s(p_t)$,

because of the weak p_t dependence of ν_n^h as shown in data at RHIC and implemented in our simulation. This also agrees with the findings in Ref. [24]. However, a decisive comparison with data again requires a good understanding of other sources of correlations.

We end with discussions on a number of issues to be improved in future studies. A detailed study of the hard-soft correlation naturally requires including a realistic medium evolution in the transverse plane through hydrodynamics [72, 73]. The linear response is a crude approximation for the soft dynamics. Moreover, such transverse expansion dynamics can also play a role in the jet quenching, in particular for higher harmonics. In this simulation, the transverse shape of the medium is frozen (matter density decreases as $1/\tau$ because of the longitudinal expansion), but in reality the eccentricities of the matter will reduce with increasing time because of the pressure gradient driven expansion (and such “self-quenching” may be a significant factor for higher harmonics) [74]. Although qualitatively the majority of jets may not experience this change very much, because the dramatic shape change happens in a relatively later stage, it is certainly interesting to explore this effect especially for harmonics other than the second harmonic, which are mostly driven by the shape fluctuations. Integration of our current jet azimuthal anisotropy study with hydrodynamics is being pursued. Furthermore, the p_t dependence of jet quenching is not implemented in the present geometric models but efforts are underway to include that. Another important uncertainty is related to possible preequilibrium energy loss, which hopefully will be better understood and estimated with improved descriptions for the preequilibrium evolution [75]. We are focusing on the geometrical information about jet anisotropy, but it is important to have a coherent understanding in terms of different variables, which requires a careful study of the hard parton energy loss for example in the near- T_c enhancement picture. Finally, we hope we have made a case here for using the hard probe as a new and sensitive tool for quantifying the initial fluctuations in heavy ion collisions and for discriminating different models for the initial conditions. Future studies along this direction will be certainly extended to hard probe of initial conditions generated from e.g., CGC-motivated models [76, 77] and their comparison with the MC Glauber model.

Acknowledgments

We thank Larry McLerran, U. Heinz, Z. Qiu, M. Gyulassy, G. Torrieri, B. Betz, A. Buzzatti, J. Jia, R. Lacey, D. Molnar, F. Wang, and S. Mukherjee for helpful communications and discussions. We are also grateful to the Institute for Nuclear Theory and the organizers of the INT Workshop on “The Ridge Correlation in High-Energy Collisions at RHIC and LHC” during which the reported research was advanced. JL thanks the RIKEN BNL Research Center for partial support. XZ was supported by the Nuclear Theory Center at Indiana University, and is now supported by the US Department of Energy under Grant No. DE-FG02-93ER-40756.

Appendix A: The structure of the simulation code

Figure 14 summarizes the overall structure of the simulation in each event. It starts with the sampling of nucleon positions in the two colliding nuclei. Based on the Glauber model, we can identify the binary collision pairs, which leads to the participant density and collision density by using proper smearing procedure. This provides the basic information for all the

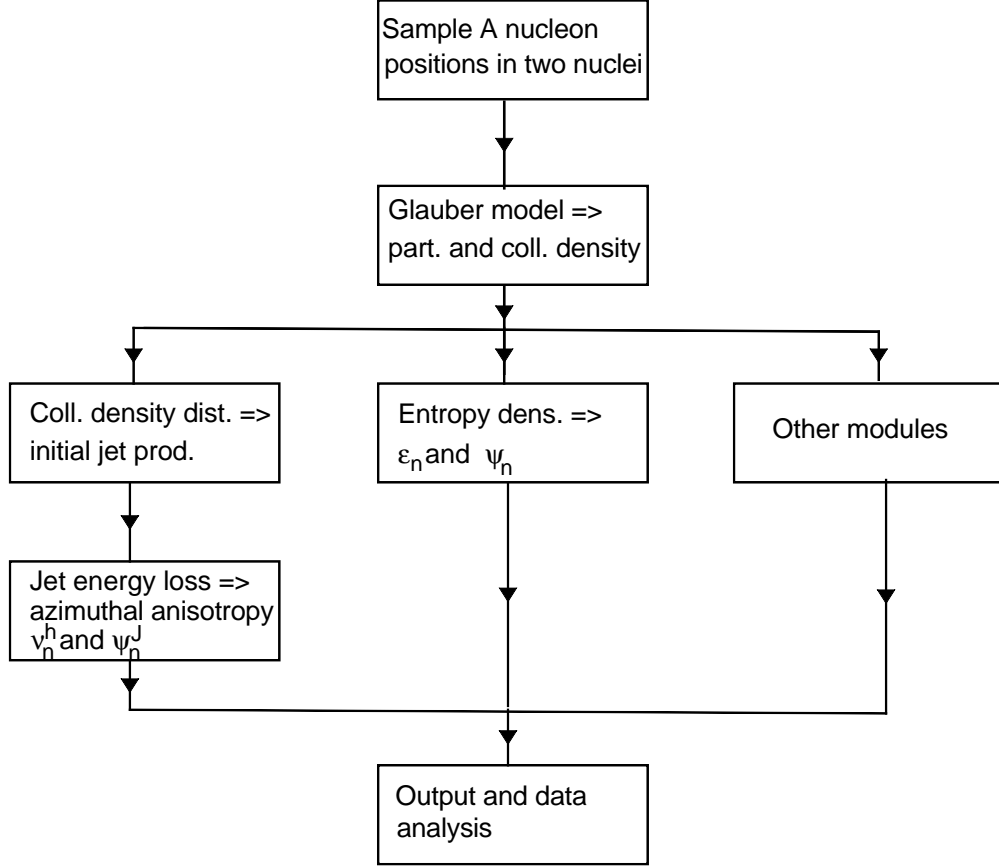


FIG. 14: The structure of the simulation code.

following calculation modules. In the jet quenching module, we calculate the azimuthal distribution of the R_{AA} as described in the text and get ν_n^h and ψ_n^J . The second module analyzes the initial entropy density, which gives ϵ_n and ψ_n . In principle other modules can be included in the code, for example the EM field calculation. Then the results from different modules are grouped together and recorded in the output file. To get an ensemble of events, the collision geometry, e.g., impact parameter for AA collision, needs to be sampled, which is not shown here.⁹ After the initialization of the collision geometry, the whole calculation shown in Fig. 14 can be carried out.

⁹ In $U-U$ collisions, the collision geometry is more complicated, requiring the sampling of impact parameter and the relative orientation of the two nuclei.

Appendix B: The formula for the triggered dihadron correlation

In this section we derive the formula for computing the triggered dihadron correlation mentioned in Sec. IV, based on the following soft and hard hadron azimuthal distributions:

$$\frac{dN^s}{d\phi^s} \sim 1 + 2 \sum_n \nu_n^s \cos[n(\phi^s - \psi_n^S)] , \quad (\text{B1})$$

$$\frac{dN^h}{d\phi^h} \sim 1 + 2 \sum_m \nu_m^h \cos[m(\phi^h - \psi_m^J)] . \quad (\text{B2})$$

According to the definition in Sec. IV, let us calculate the following:

$$\int_{\mathcal{R}} d\phi^s d\phi^h \frac{dN^s}{d\phi^s} \frac{dN^h}{d\phi^h} \delta(\phi^s - \phi^h - \Delta\phi) \sim 1 + C(\Delta\phi) \equiv 1 + 2 \sum_n \nu_n^s \tilde{\nu}_n^h \cos(n\Delta\phi) . \quad (\text{B3})$$

Here \mathcal{R} is composed of four different pieces: $\phi_\alpha - \phi_\beta \leq \phi^h - \psi^{\text{EP}} \leq \phi_\alpha + \phi_\beta$ (ϕ_α is in the first quadrant) and the other three with $\phi_\alpha \rightarrow -\phi_\alpha, \pi + \phi_\alpha, \pi - \phi_\alpha$. We keep track of the difference between ψ_n^S (ψ_n^J) and ψ^{EP} , which is different from Ref. [54]. By using Eqs. (B2) and (B1), we get

$$\begin{aligned} & \tilde{\nu}_n^h \left[1 + 2 \sum_{K=2,4,\dots} \nu_K^h \cos(K\Delta\psi_K^J) t_K \right] \\ &= \delta_{n,\text{even}} \cos(n\Delta\psi_n^S) t_n \\ & \quad + \sum_{\substack{m+n=\text{even} \\ m,n}} \nu_m^h t_{m+n} \cos[m\Delta\psi_m^J + n\Delta\psi_n^S] \\ & \quad + \sum_{\substack{m-n=\text{even} \\ m,n}} \nu_m^h t_{m-n} \cos[m\Delta\psi_m^J - n\Delta\psi_n^S] \\ &= \nu_n^h \cos[n(\Delta\psi_n^J - \Delta\psi_n^S)] + \delta_{n,\text{even}} \cos(n\Delta\psi_n^S) t_n \\ & \quad + \sum_{K=2,4,\dots} \nu_{n+K}^h t_K \cos[(n+K)\Delta\psi_{n+K}^J - n\Delta\psi_n^S] \\ & \quad + \sum_{K=2,4,\dots} \nu_{|n-K|}^h t_K \cos[(n-K)\Delta\psi_{|n-K|}^J - n\Delta\psi_n^S] . \end{aligned} \quad (\text{B4})$$

In the above expression, $\Delta\psi_n^J \equiv \psi_n^J - \psi^{\text{EP}}$; $\Delta\psi_n^S \equiv \psi_n^S - \psi^{\text{EP}}$; $t_n \equiv \frac{\sin(n\phi_\beta)}{n\phi_\beta} \cos(n\phi_\alpha)$. If we assume all the reference angles ψ_n^S and ψ_n^J are exactly correlated with ψ^{EP} , the above formula would become the one in Ref. [54]. To compare with the data, we need to average $C(\Delta\phi)$ over many events, i.e., $\langle C(\Delta\phi) \rangle$. In principle, $C(\Delta\phi)$ should also have $\sin(n\Delta\phi)$ components, but their amplitudes should be very small with many events averaged. [We will simply use $C(\Delta\phi)$ as $\langle C(\Delta\phi) \rangle$ from now on.]

Appendix C: Discussion on the near- T_c enhancement and the trace anomaly

We discuss here the possible connection between the near- T_c enhancement of jet-medium interaction and the QCD trace anomaly $(\epsilon - 3p)/T^4$ (with ϵ, p, T the energy density, pressure

and temperature) which as an interaction measure also develops a strong near- T_c peak as shown by lattice QCD simulations [78, 79]. One may naturally ask whether these two non-perturbative effects near T_c could share a common underlying picture. We notice that there have been attempts [56] to develop nonconformal holographic models based on gauge/gravity duality that can mimic the QCD trace anomaly well but face tensions in describing jet quenching phenomenon. In this appendix, we will show that the near- T_c enhancement and the trace anomaly may be consistently described together by a plasma of magnetic monopoles based on the “magnetic scenario” in [15, 16, 80, 81].

We consider QCD near- T_c plasma as an ensemble of thermal magnetic monopoles with certain density $n_m(T)$ and effective mass $M_m(T)$. Let us first compute the contribution to trace anomaly from this magnetic component. As a crude approximation let us first neglect the potential energy and express the trace anomaly through the density, i.e.,

$$\frac{\epsilon - 3p}{T^4} = \frac{n_m}{T^3} \chi_M \quad (\text{C1})$$

with the dimensionless coefficient χ_M defined as:

$$\chi_M \equiv \left\langle \frac{\tilde{M}^2}{\sqrt{x^2 + \tilde{M}^2}} \right\rangle = \frac{\int_0^\infty \frac{x^2 dx}{\exp(\sqrt{x^2 + \tilde{M}^2}) - 1} \frac{\tilde{M}^2}{\sqrt{x^2 + \tilde{M}^2}}}{\int_0^\infty \frac{x^2 dx}{\exp(\sqrt{x^2 + \tilde{M}^2}) - 1}} \quad (\text{C2})$$

In the above the thermal monopole mass $\tilde{M} = M_m/T$ is about 1.5 – 2 when close to T_c [82, 83], which corresponds to $\chi_M \approx 0.7 - 1.1$. We therefore have roughly the relation

$$\frac{\epsilon - 3p}{T^4} \approx (0.7 - 1.1) \times \frac{n_m}{T^3} \quad (\text{C3})$$

Now the monopole density close to T_c , according to lattice results and model studies [16, 80–83], is about $n_m/T^3 \approx 2 - 3$, so we get an estimate of the monopole contribution to trace anomaly near T_c of about

$$\frac{\epsilon - 3p}{T^4} \approx 1.4 - 3.3 \quad (\text{C4})$$

Note that the peak value of trace anomaly found from lattice simulations is about $\frac{(\epsilon - 3p)}{T^4}|_{peak} \approx 4$ [78, 79], so the above contribution is very consistent with lattice data and actually is the dominant part. The mild difference may be made up from the interaction among monopoles: according to the analysis in [15, 82] the interaction potential energy is comparable with the kinetic, so could contribute a similar amount to the trace anomaly. We also note that the rapid decrease of trace anomaly with increasing temperature can be understood from the rapidly dropping density n_m/T^3 for $T > T_c$.

Let us now turn to the discussion of the jet-medium interaction within the same magnetic scenario. With a picture similar to the GLV model for jet energy loss [1], while replacing the Coulomb electric scattering centers by the magnetic ones in the near- T_c plasma, we expect roughly the amount of medium kick received by a penetrating electric jet to scale as

$$\sim \alpha_E(T) \alpha_M(T) n_m(T) \quad (\text{C5})$$

While the electric coupling α_E and magnetic coupling α_M both depend on temperature scale, their product has to be unity as per the famous Dirac condition, i.e., $\alpha_E(T)\alpha_M(T) = 1$. Therefore, we see that if we normalize the medium kick by the entropy density at the same temperature, we will get

$$\kappa \sim \frac{\alpha_E(T)\alpha_M(T)n_m(T)}{s(T)} = \frac{n_m/T^3}{s/T^3} \quad (\text{C6})$$

Again the monopole density n_m/T^3 strongly peaks at T_c [16, 82, 83] while s/T^3 relatively slowly decreases from high temperature to low temperature [78, 79]. As a result the normalized jet-medium interaction strength κ develops a strong near- T_c enhancement. To make a more quantitative statement, let us compare the κ at two temperatures: from $1.5T_c$ to T_c the monopole density increases by a factor of ~ 3 while the entropy density s/T^3 decreases by a factor of ~ 2 , and therefore the κ increases by a factor of ~ 6 from $1.5T_c$ down to T_c which is well in accord with the assumed enhancement in the NTcE model.

To sum up the above qualitative discussions and estimates, we see that the presence of an emergent monopole plasma near- T_c with the density and thermal mass indicated by lattice and model studies, can consistently describe the strong near T_c peaks in both the trace anomaly and the jet-medium interaction.

Appendix D: An estimate of average opaqueness from RHIC to LHC

In this part we make a simple estimate, in the NTcE model, of the evolution of the average opaqueness of the fireball from RHIC to LHC. The hot medium created in heavy ion collisions is neither homogeneous nor static, and therefore one can only talk about the opaqueness of the fireball created in the collision on an average sense, i.e., averaging both over the spatial distribution and the time evolution. For simplicity let us consider the perfectly central collision with $b = 0$. We will use this case as an indicator of the opaqueness evolution with collision beam energies. The average opaqueness seen by a jet going through the medium along a particular path P can be estimated as follows:

$$\langle \kappa[s(l)] \rangle_P = \frac{\int_P \kappa[s(l)] s(l) l dl}{\int_P s(l) l dl} \quad (\text{D1})$$

Note that, even for the same geometry and same jet path in fireballs created at different collision energies, the $s(l)$ will be very different and the convolution with $\kappa[s(l)]$ is rather nontrivial due to the peculiar near- T_c enhancement form in Eq. (5). This is of course further subject to averaging over paths, i.e., over all initial jet spots weighed by collision density as well as all possible jet directions. We will use a simple optical Glauber model (with the same parameter sets as in the previous MC Glauber simulations) to evaluate this average. Note that the longitudinal boost-invariant expansion effect is also included as in the previous MC calculations, i.e., the density $s(l)$ on a specific point of the path is really a function of both l and time t .

To give a quick idea, we can simply consider a jet initiating right from the center $\mathbf{r}_\perp = 0$: with this simplest path we can easily obtain $\langle \kappa \rangle_{\text{RHIC}} : \langle \kappa \rangle_{\text{LHC}} \approx 1 : 0.75$. Clearly we see a shift toward less opaqueness as a consequence of two factors: the near- T_c structure of $\kappa(s)$ and the shift to higher density matter at LHC. In contrast, all models with a constant κ will see no change in the opaqueness from RHIC to LHC. A full evaluation averaging over

initial jet spots and paths with fluctuating initial condition gives the following evolution of average opaqueness:

$$\langle \kappa \rangle_{\text{RHIC}} : \langle \kappa \rangle_{\text{LHC}} \approx 1 : 0.72 \quad (\text{D2})$$

We note this is not only qualitatively but quantitatively in agreement with the earlier analysis in [4] which found that in order to describe the LHC R_{AA} data the jet-medium coupling parameter κ (which is a constant in the model of [4]) has to be reduced by a factor $\sim 30\%$ from the RHIC value in the same model. What we want to emphasize here is that such a reduction of (average) jet-medium interaction implied by data from RHIC to LHC is naturally borne out from the strong near- T_c enhancement of jet-medium interaction.

-
- [1] M. Gyulassy, I. Vitev, X. -N. Wang, B. -W. Zhang, *Quark Gluon Plasma 3*, Edited by R.C. Hwa and X.-N. Wang, World Scientific, Singapore [arXiv: nucl-th/0302077]; P. Jacobs, X. -N. Wang, Prog. Part. Nucl. Phys. **54**, 443-534 (2005). R. J. Fries, C. Nonaka, Prog. Part. Nucl. Phys. **66**, 607-660 (2011). J. Casalderrey-Solana, H. Liu, D. Mateos, K. Rajagopal, U. A. Wiedemann, [arXiv:1101.0618 [hep-th]].
 - [2] J. Liao, AIP Conf. Proc. **1441**, 874 (2012) [arXiv:1109.0271 [nucl-th]].
 - [3] W. A. Horowitz, M. Gyulassy, Nucl. Phys. A **872**, 265 (2011) [arXiv:1104.4958 [hep-ph]].
 - [4] B. Betz and M. Gyulassy, Phys. Rev. C **86**, 024903 (2012) arXiv:1201.0281 [nucl-th].
 - [5] X. Zhang and J. Liao, Phys. Lett. **B** 713, 35 (2012).
 - [6] M. Gyulassy, I. Vitev and X. N. Wang, Phys. Rev. Lett. **86**, 2537 (2001).
 - [7] X. N. Wang, Phys. Rev. C **63**, 054902 (2001).
 - [8] E. V. Shuryak, Phys. Rev. **C66**, 027902 (2002).
 - [9] A. Drees, H. Feng, J. Jia, Phys. Rev. **C71**, 034909 (2005).
 - [10] J. Jia, W. A. Horowitz and J. Liao, Phys. Rev. C **84**, 034904 (2011).
 - [11] R. Rodriguez, R. J. Fries and E. Ramirez, Phys. Lett. B **693**, 108 (2010).
 - [12] T. Renk, Phys. Rev. C **85**, 044903 (2012).
 - [13] T. Renk, H. Holopainen, J. Auvinen and K. J. Eskola, Phys. Rev. C **85**, 044915 (2012).
 - [14] J. Liao, E. Shuryak, Phys. Rev. Lett. **102**, 202302 (2009).
 - [15] J. Liao, E. Shuryak, Phys. Rev. **C75**, 054907 (2007); Phys. Rev. Lett. **101**, 162302 (2008); *ibid* **109**, 152001 (2012) arXiv:1206.3989 [hep-ph].
 - [16] J. Liao, E. Shuryak, Phys. Rev. **D82**, 094007 (2010); Phys. Rev. **C77**, 064905 (2008); Nucl. Phys. **A775**, 224-234 (2006).
 - [17] B. Alver and G. Roland, Phys. Rev. C **81**, 054905 (2010) [Erratum-*ibid.* C **82**, 039903 (2010)].
 - [18] R. Lacey [for the PHENIX Collaboration], J. Phys. G **38**, 124048 (2011).
 - [19] P. Sorensen [STAR Collaboration], J. Phys. G **38**, 124029 (2011).
 - [20] J. F. Grosse-Oetringhaus, J. Phys. G **38**, 124028 (2011).
 - [21] J. Jia, J. Phys. G **38**, 124012 (2011).
 - [22] W. Li [CMS Collaboration], J. Phys. G **38**, 124027 (2011).
 - [23] B. H. Alver, C. Gombeaud, M. Luzum and J. -Y. Ollitrault, Phys. Rev. C **82**, 034913 (2010).
 - [24] Matthew Luzum, Phys. Lett. B **696**, 499 (2011).
 - [25] R. S. Bhalerao, M. Luzum and J. -Y. Ollitrault, Phys. Rev. C **84**, 034910 (2011).
 - [26] M. Luzum, J. Phys. G **38**, 124026 (2011).

- [27] P. Sorensen, arXiv:0811.2959 [nucl-ex]. A. Mocsy and P. Sorensen, arXiv:1008.3381 [hep-ph]. P. Sorensen, B. Bolliet, A. Mocsy, Y. Pandit and N. Pruthi, Phys. Lett. B **705**, 71 (2011).
- [28] D. Teaney and L. Yan, Phys. Rev. C **83**, 064904 (2011).
- [29] Z. Qiu and U. W. Heinz, Phys. Rev. C **84**, 024911 (2011).
- [30] Z. Qiu, C. Shen and U. W. Heinz, Phys. Lett. B **707**, 151 (2012).
- [31] P. Staig and E. Shuryak, Phys. Rev. C **84**, 034908 (2011). P. Staig and E. Shuryak, Phys. Rev. C **84**, 044912 (2011).
- [32] J. Takahashi, B. M. Tavares, W. L. Qian, R. Andrade, F. Grassi, Y. Hama, T. Kodama and N. Xu, Phys. Rev. Lett. **103**, 242301 (2009).
- [33] B. Schenke, S. Jeon and C. Gale, Phys. Rev. Lett. **106**, 042301 (2011).
- [34] J. Xu and C. M. Ko, Phys. Rev. C **83**, 021903 (2011).
- [35] G. -Y. Qin, H. Petersen, S. A. Bass and B. Muller, Phys. Rev. C **82**, 064903 (2010).
- [36] G. -L. Ma and X. -N. Wang, Phys. Rev. Lett. **106**, 162301 (2011).
- [37] R. P. G. Andrade, F. Grassi, Y. Hama, and W. -L. Qian, Phys. Lett. B **712**, 226 (2012).
- [38] J. Jia, R. Wei, Phys. Rev. C **82**, 024902 (2010).
- [39] B. Betz, M. Gyulassy and G. Torrieri, Phys. Rev. C **84**, 024913 (2011). B. Betz, M. Gyulassy, G. Torrieri, J. Phys. G **38**, 124153 (2011) [arXiv:1106.4564 [nucl-th]].
- [40] A. Adare *et al.* [PHENIX Collaboration], Phys. Rev. Lett. **107**, 252301 (2011).
- [41] B. Abelev *et al.* [ALICE Collaboration], arXiv:1205.5761 [nucl-ex].
- [42] S. Chatrchyan *et al.* [CMS Collaboration], Eur. Phys. J. C **72** 2012 (2012); Phys. Rev. Lett. **109**, 022301 (2012) [arXiv:1204.1850 [nucl-ex]].
- [43] G. Aad *et al.* [ATLAS Collaboration], Phys. Rev. C **86**, 014907 (2012); Phys. Lett. B **707**, 330 (2012).
- [44] X. Zhang and J. Liao, arXiv:1208.6361 [nucl-th].
- [45] H. Zhang, J. F. Owens, E. Wang and X. -N. Wang, Phys. Rev. Lett. **98**, 212301 (2007).
- [46] T. Renk and K. J. Eskola, Phys. Rev. C **75**, 054910 (2007).
- [47] B. I. Abelev *et al.* [STAR Collaboration], Phys. Rev. C **80**, 064912 (2009). M. M. Aggarwal *et al.* [STAR Collaboration], Phys. Rev. C **82**, 024912 (2010). H. Agakishiev *et al.* [STAR Collaboration], arXiv:1010.0690 [nucl-ex]. G. Agakishiev *et al.* [STAR Collaboration], Phys. Rev. C **85**, 014903 (2012) [arXiv:1110.5800 [nucl-ex]].
- [48] E. V. Shuryak, Phys. Rev. C **76**, 047901 (2007).
- [49] A. Majumder, B. Muller and S. A. Bass, Phys. Rev. Lett. **99**, 042301 (2007).
- [50] A. Dumitru, F. Gelis, L. McLerran and R. Venugopalan, Nucl. Phys. A **810**, 91 (2008).
- [51] J. Adams *et al.* [STAR Collaboration], Phys. Rev. Lett. **93**, 252301 (2004).
- [52] A. Feng, J. Phys. G **35**, 104082 (2008).
- [53] H. Agakishiev *et al.* [STAR Collaboration], arXiv:1010.0690 [nucl-exp] (2010).
- [54] J. Bielcikova, S. Esumi, K. Filimonov, S. Voloshin, and J. P. Wurm, Phys. Rev. C **69**, 021901(R) (2004).
- [55] M. Gyulassy, private communication.
- [56] A. Ficnar, J. Noronha and M. Gyulassy, arXiv:1208.0305 [hep-ph]; J. Phys. G **38**, 124176 (2011); Nucl. Phys. A **855**, 372 (2011). J. Noronha, Phys. Rev. D **81**, 045011 (2010).
- [57] B. G. Zakharov, JETP Lett. **93**, 683 (2011).
- [58] R. A. Lacey, N. N. Ajitanand, J. M. Alexander, J. Jia and A. Taranenko, arXiv:1202.5537 [nucl-ex]; arXiv:1203.3605 [nucl-ex].
- [59] A. Majumder, Phys. Rev. C **87**, 034905 (2013) [arXiv:1202.5295 [nucl-th]].
- [60] M. L. Miller, K. Reygers, S. J. Sanders, and P. Steinberg, Annu. Rev. Nucl. Part. Sci. **57** 205

- (2007)
- [61] Ulrich Heinz and J. S. Moreland, Phys. Rev. C **84**, 054905 (2011).
 - [62] Tetsufumi Hirano, Pasi Huovinen, and Yasushi Nara, Phys. Rev. C **83**, 021902(R) (2011)
 - [63] Z. Qiu, private communication.
 - [64] Chun Shen, Ulrich Heinz, Pasi Huovinen, and Huichao Song, Phys. Rev. C **84**, 044903 (2011).
 - [65] S. S. Adler *et al.* [PHENIX Collaboration], Phys. Rev. **C76**, 034904 (2007).
 - [66] K. Aamodt *et al.* [ALICE Collaboration], Phys. Lett. B **696**, 30 (2011).
 - [67] François Arleo, David d’Enterria, and Andre S. Yoon, JHEP **06** 035 (2010).
 - [68] J. Jia, [arXiv:1203.3265] (2012).
 - [69] H. Agakishiev *et al.*, (STAR collaboration), arXiv:1010.0690.
 - [70] B. Betz, J. Noronha, G. Torrieri, M. Gyulassy and D. H. Rischke, Phys. Rev. Lett. **105**, 222301 (2010).
 - [71] A. Bzdak, V. Koch and J. Liao, Lect. Notes Phys. *Strongly interacting matter in magnetic fields*, edited by D. Kharzeev, K. Landsteiner, A. Schmitt, and H.-U. Yee, Springer [arXiv:1207.7327 [nucl-th]]; Phys. Rev. C **81**, 031901 (2010).
 - [72] T. Renk, J. Ruppert, C. Nonaka and S. A. Bass, Phys. Rev. C **75**, 031902 (2007).
 - [73] S. A. Bass, C. Gale, A. Majumder, C. Nonaka, G. -Y. Qin, T. Renk and J. Ruppert, Phys. Rev. C **79**, 024901 (2009).
 - [74] D. Molnar and D. Sun, arXiv:1209.2430 [nucl-th].
 - [75] J. -P. Blaizot, F. Gelis, J. -F. Liao, L. McLerran and R. Venugopalan, Nucl. Phys. A **873**, 68 (2012).
 - [76] D. Kharzeev and M. Nardi, Phys. Lett. B **507**, 121 (2001).
 - [77] B. Schenke, P. Tribedy and R. Venugopalan, Phys. Rev. C **86**, 034908 (2012) [arXiv:1206.6805 [hep-ph]].
 - [78] S. Borsanyi, G. Endrodi, Z. Fodor, A. Jakovac, S. D. Katz, S. Krieg, C. Ratti and K. K. Szabo, JHEP **1011**, 077 (2010). C. Ratti, in Proceedings of Quark Matter 2012.
 - [79] M. Cheng, S. Ejiri, P. Hegde, F. Karsch, O. Kaczmarek, E. Laermann, R. D. Mawhinney and C. Miao *et al.*, Phys. Rev. D **81**, 054504 (2010). A. Bazavov, in Proceedings of Quark Matter 2012.
 - [80] M. N. Chernodub and V. I. Zakharov, Phys. Rev. Lett. **98**, 082002 (2007).
 - [81] C. Ratti and E. Shuryak, Phys. Rev. D **80**, 034004 (2009).
 - [82] A. D’Alessandro, M. D’Elia and E. V. Shuryak, Phys. Rev. D **81**, 094501 (2010). A. D’Alessandro and M. D’Elia, Nucl. Phys. B **799**, 241 (2008).
 - [83] V. G. Bornyakov, A. G. Kononenko and A. G. Kononenko, Phys. Rev. D **86**, 074508 (2012) [arXiv:1111.0169 [hep-lat]]. V. G. Bornyakov and V. V. Braguta, Phys. Rev. D **85**, 014502 (2012).

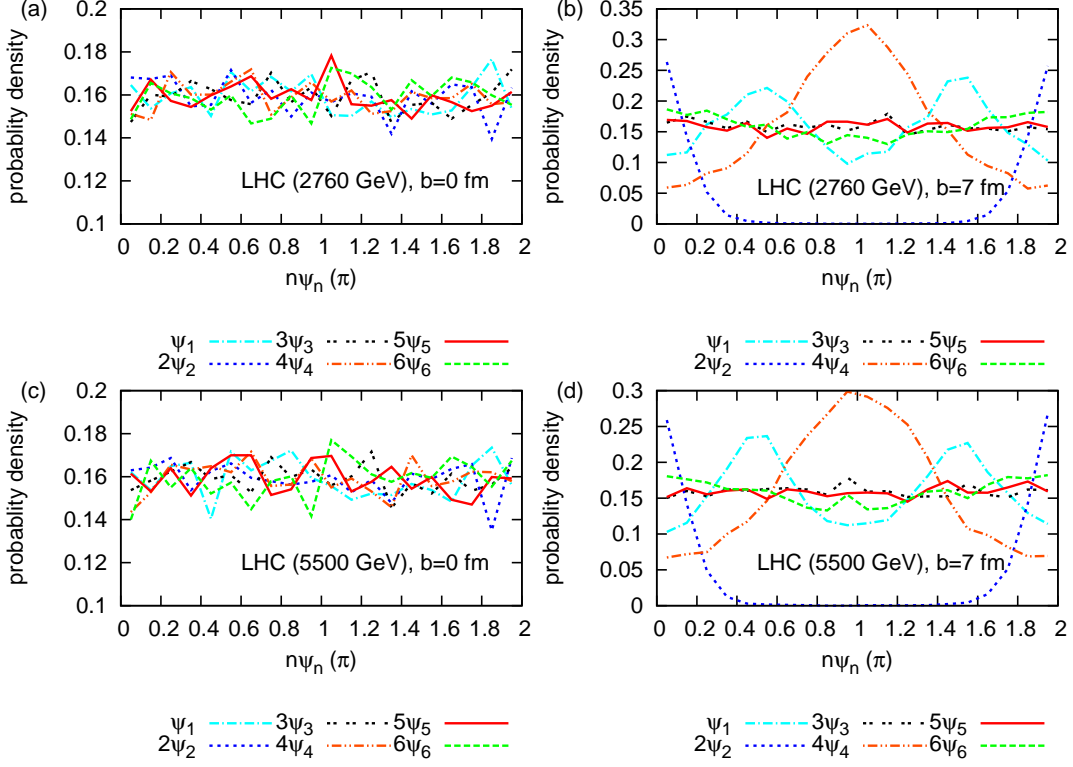


FIG. 15: (Color online). The distribution of ψ_n with $b = 0, 7$ fm at LHC ($\sqrt{s} = 2760, 5500$ GeV). For $b = 7$ fm, $(2\psi_2)$'s probability density is scaled down by a factor 0.3.

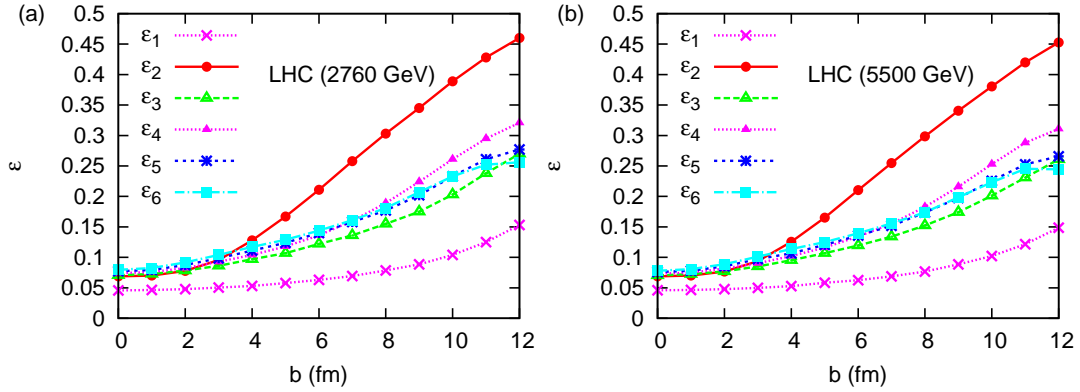


FIG. 16: (Color online). The b dependence of ϵ_n at LHC ($\sqrt{s} = 2760, 5500$ GeV).

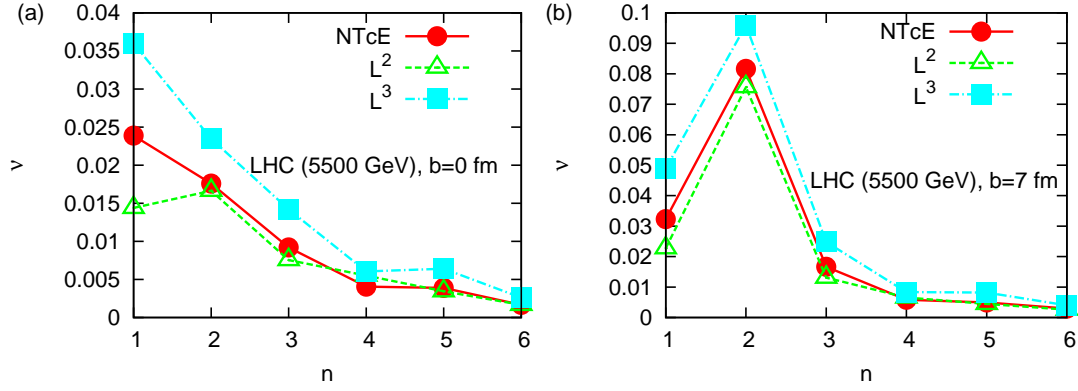


FIG. 17: (Color online). The spectrum of ν_n^h for LHC ($\sqrt{s} = 5500$ GeV) at $b = 0, 7$ fm, based on three different models.

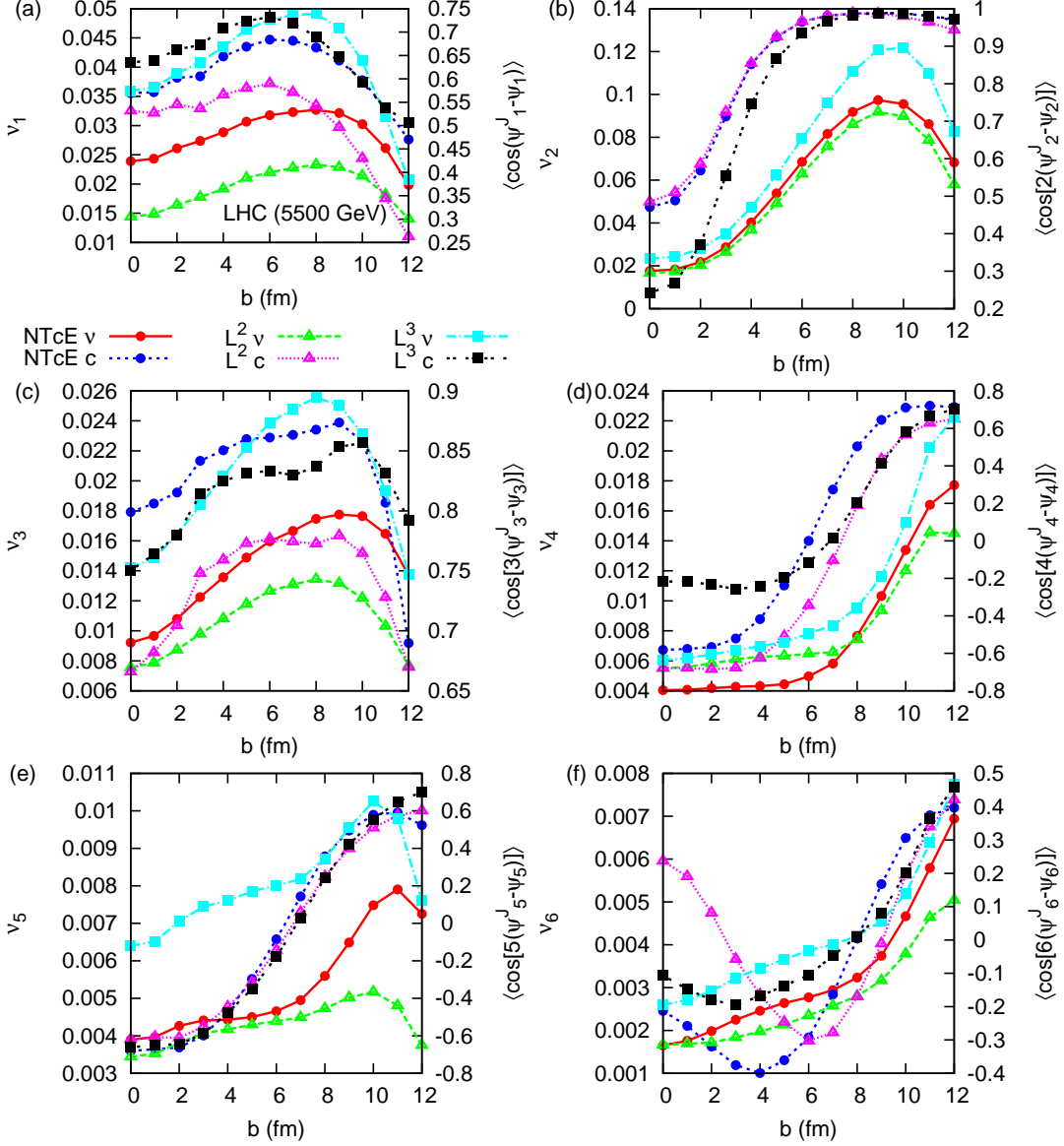


FIG. 18: (Color online). The b dependence of ν_n^h and $\langle \cos[n(\psi_n^J - \psi_n)] \rangle$ for LHC ($\sqrt{s} = 5500$ GeV) based on three different models.

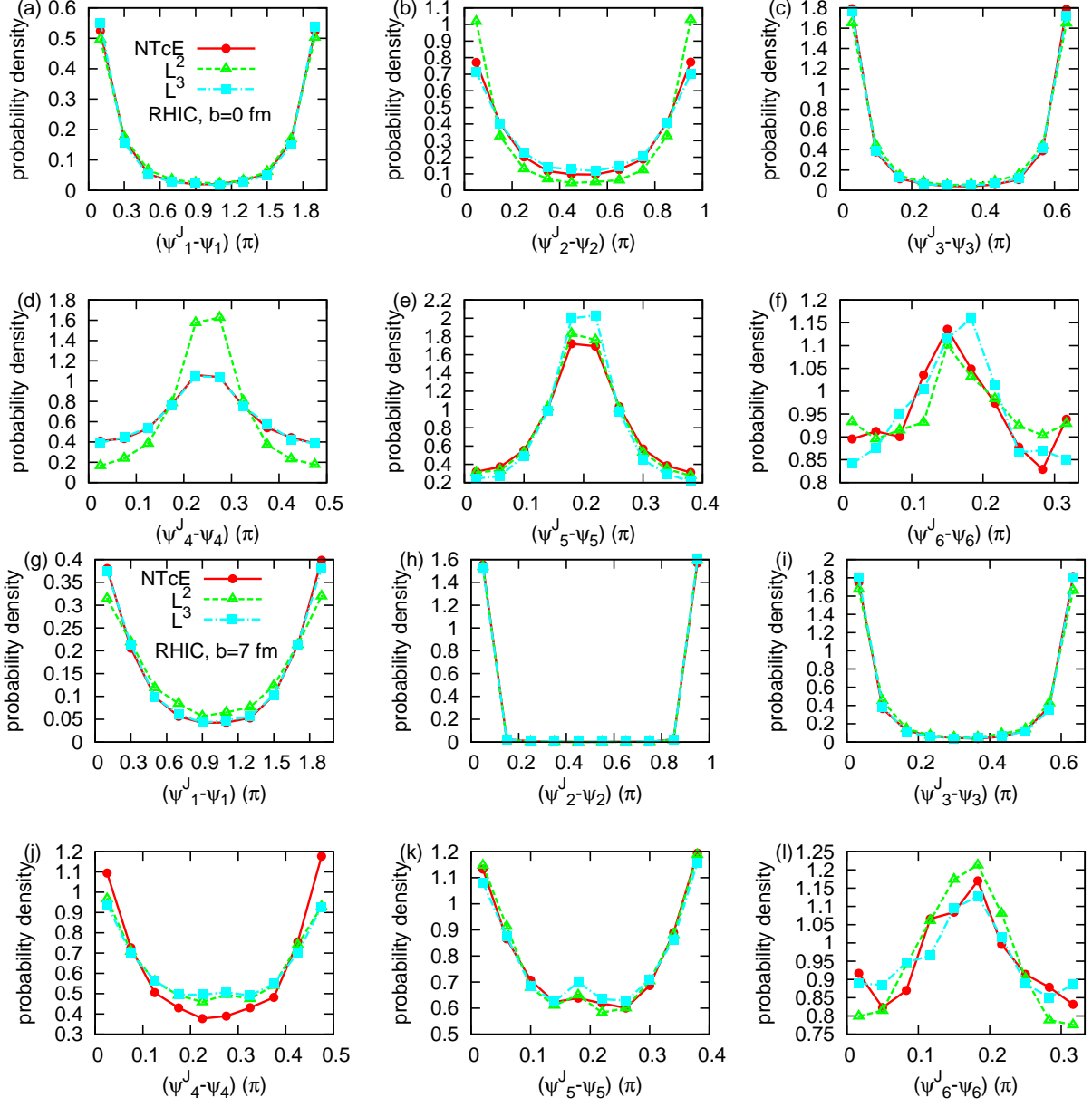


FIG. 19: (Color online). The distribution of $\psi_n^J - \psi_n$ for RHIC ($\sqrt{s} = 200$ GeV) at $b = 0, 7$ fm, based on three different models.

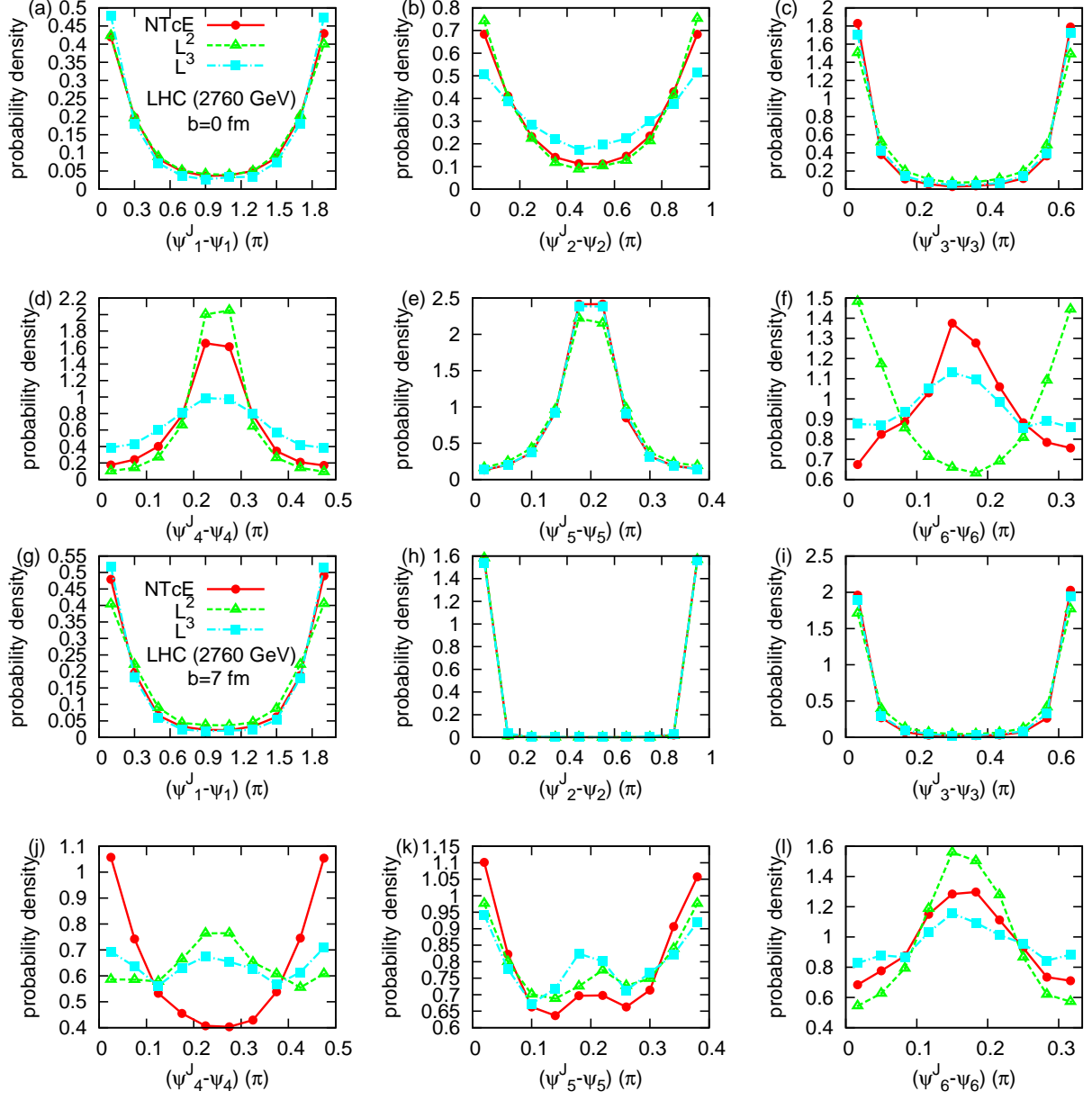


FIG. 20: (Color online). The distribution of $\psi_n^J - \psi_n$ for LHC ($\sqrt{s} = 2760$ GeV) at $b = 0, 7$ fm, based on three different models.

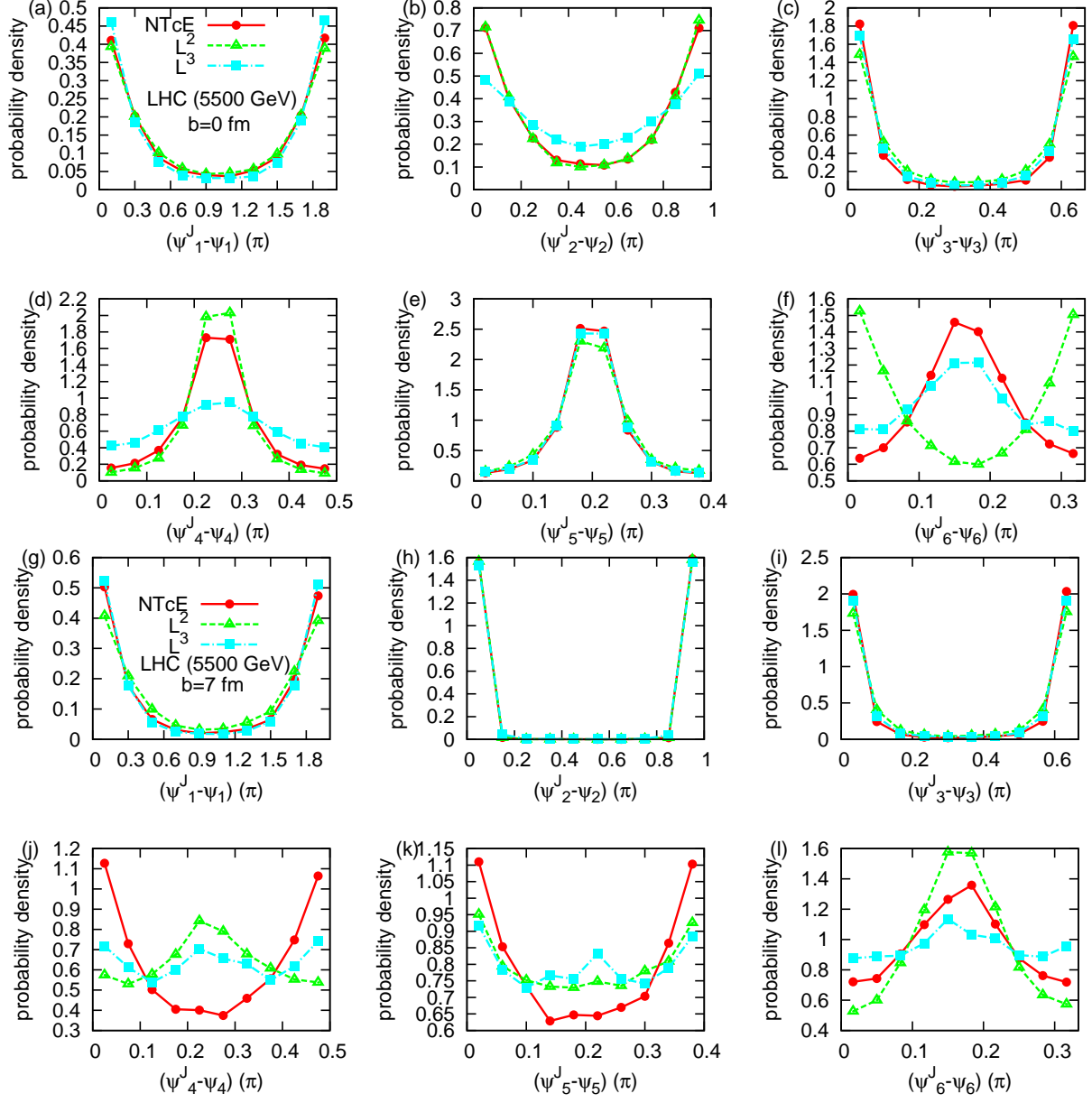


FIG. 21: (Color online). The distribution of $\psi_n^J - \psi_n$ for LHC ($\sqrt{s} = 5500$ GeV) at $b = 0, 7$ fm, based on three different models.